Supplementary Material (Text, Tables and Figures)

Effects of Environmental and Management Factors on Worldwide Maize and Soybean Yields over the 20th and 21st Centuries

Tzu-Shun Lin[1], Yang Song[2], Atul K Jain[1*], Peter Lawrence[3], and Haroon S Kheshgi[4]

[1]Department of Atmospheric Sciences, University of Illinois, Urbana, IL 61801, USA

[2] Department of Hydrology and Atmospheric Sciences, University of Arizona, Tucson, AZ, 85721, USA

[3]National Center for Atmospheric Research, Boulder, CO 80305, USA

[4]ExxonMobil Research and Engineering Company, Annandale, NJ 08801, USA

Supplementary Text Sections

Text S1. Bias Correction of Future Climate

The bias correction method proposed by Hawkins et al. (2013) is used in this study to correct the six atmospheric variables, including downward shortwave and longwave radiation, surface pressure, wind speed, surface temperature and specific humidity from CESM outputs. This method considers the mean and variability differences between CRU-NCEP reanalysis and CESM output between year 2006 and 2016:

$$\mathrm{T_{cor}} = \overline{\mathrm{T_{obs}}} + \frac{\sigma_{\mathrm{obs}}}{\sigma_{\mathrm{ref}}} \times (\mathrm{T_{raw}} - \overline{\mathrm{T_{ref}}}) \qquad \text{(SE1)}$$

where $\mathrm{T_{cor}}$ is bias-corrected CESM variables, $\overline{\mathrm{T_{obs}}}$ represents mean CRU-NCEP outputs from the historical reference period, $\mathrm{T_{raw}}$ is raw datasets from historical or future CESM variables, $\overline{\mathrm{T_{ref}}}$ is a mean CESM output from the same historical reference period, σ_{obs} and σ_{ref} represents the standard deviation in the reference period of CRU-NCEP and CESM variables, respectively. The data are corrected every six hour averaged from eleven years. This method not only considers the mean values but also involves the temporal variance of the model outputs in accordance with the observations (Ho et al., 2012).

The correction of future precipitation is calculated using the following equation:

$$\mathrm{P_{cor}} = \mathrm{P_{raw}} \times \frac{\overline{\mathrm{P_{obs,m}}}}{\overline{\mathrm{P_{raw,m}}}} \qquad \text{(SE2)}$$

where$\mathrm{P_{cor}}$ is bias-corrected model precipitation, $\mathrm{P_{raw}}$ stands for uncorrected corresponding precipitation, $\frac{\overline{\mathrm{P_{obs,m}}}}{\overline{\mathrm{P_{raw,m}}}}$ is the ratio of monthly mean precipitation from CRU-NCEP to that from CESM for the same reference period (Déqué et al., 2007). This method reduces mean biases between models and observations; however, it does not take coefficient of variance of the modeled precipitation into account.

Text S2. Estimation of Crop Specific Harvested Area for Irrigated and Non-Irrigated Conditions

LUH2 provides the 5-category cropland distributions (C3 annual crops, C3 perennial crops, C4 annual crops, C4 perennial crops, and C3 nitrogen-fixing crops) during the historic period 1850-2015 and 2016-2100 for SSP scenarios (Hurtt et al., in preparation), while both MIRCA2000 (Portmann et al., 2010) and M3 (Monfreda et al., 2008) data set include crop-specific cropland areas and harvested areas, but for the year 2000. The process for generating crop-specific harvested areas consisted of four steps (Eq. S18): (i) since the LUH2 cropland area amount is not the same as for M3 data in year 2000, we divide the M3 data by LUH2 to calculate the bias factor ($\frac{\mathrm{M3}_a}{\mathrm{LUH2}_a}$), (ii) calculate the ratio of crop-specific harvested areas to cropland areas from M3 data set ($\frac{\mathrm{M3}_o}{\mathrm{M3}_a}$), (iii) calculate the ratio of crop-specific rainfed and irrigated harvested areas to the crop-specific harvested areas from MIRCA2000 (apply for the period 850-2015) or LUH2 (apply for scenarios for the period 2016-2100) ($\frac{\mathrm{FR}_{i,o}}{\mathrm{FR}_o}$), (iv) multiplying each factor from step (i), (ii), (iii) by time-varying LUH2 cropland areas to calculate fraction of crop-specific; irrigated or rainfed harvested areas over 0.5 degree grid cell areas from year 850 to 2100.

$$\mathrm{Crop}_{i,o} = \frac{\mathrm{M3}_a}{\mathrm{LUH2}_a} \times \frac{\mathrm{M3}_o}{\mathrm{M3}_a} \times \frac{\mathrm{FR}_{i,o}}{\mathrm{FR}_o} \times \frac{\mathrm{LUH2}_a}{\mathrm{Grid}} \qquad \text{(SE3)}$$

where subscripts a: total cropland areas; i: irrigated or rainfed conditions; o: crop-specific types; $\mathrm{FR}_{i,o}$: crop-specific irrigated or rainfed harvested areas from MIRCA2000 data; FR_o:crop-specific total (rainfed plus irrigated) harvested areas from MIRCA2000 data; $\mathrm{M3}_o$: crop-specific total (rainfed plus irrigated) harvested areas from M3 data; $\mathrm{M3}_a$:cropland areas from M3 data; $\mathrm{LUH2}_a$: cropland areas from LUH2 data; Grid : 0.5 degree grid cell areas.

To compare the annual maize and soybean yields with published datasets, the simulated yields are weighted to combine yields under fully irrigated assuming no water stress and rainfed (no irrigation) conditions to grid-cell levels, regional as well as global scales using the following equation.

$$\mathrm{Yield}_\mathrm{F} = \frac{\mathrm{Yield}_\mathrm{ir} \times \mathrm{harea}_\mathrm{ir} + \mathrm{Yield}_\mathrm{rf} \times \mathrm{harea}_\mathrm{rf}}{\mathrm{harea}_\mathrm{ir} + \mathrm{harea}_\mathrm{rf}} \qquad \text{(SE4)}$$

where $\mathrm{Yield}_\mathrm{F}$ represents crop-specific yields (t/ha) by aggregating yields with irrigated areas and rainfed areas; $\mathrm{Yield}_\mathrm{ir}$ is yield (t/ha) produced from simulations with applying irrigation; $\mathrm{Yield}_\mathrm{rf}$ is yield (t/ha) produced from simulations without irrigation (rainfed conditions); $\mathrm{harea}_\mathrm{ir}$ is irrigated harvested areas (ha), and $\mathrm{harea}_\mathrm{rf}$ is rainfed harvested areas (ha).

Text S3. Estimation of Crop Specific N Inputs at Spatial Scale

We use crop-specific spatially resolved M3 data (Mueller et al., 2012) for N input (sum of N fertilizer, deposition, and manure), which is available for the year 2000, and spatial and temporal varying N fertilizer input data of LUH2 (Hurtt et al., in preparation) for C3 and C4 crops. The LUH2 data is available for the historical time period and for the two future scenarios. We first separate the of M3 N input data into fertilizer, deposition, and manure by using N input data of Liu et al. (2010), which provides the percentage contribution of fertilizer, deposition, and manure to the total N input at a continental scale. We apply these percentages to M3 N input data to obtain the N fertilizer, deposition, and manure for each crop of M3 at a spatial scale. Then we use following procedure to obtain the spatial distribution of N fertilizer amount: (1) divide the crop-specific N fertilizer rate to total N fertilizer rate from M3 cropland to calculate the fraction of fertilizer amount (FFA) for individual crop, (2) divide the total M3 fertilizer amount to that of the LUH2 amount to calculate the bias factor (BF), and (3) multiply LUH2-based time varying values of fertilizer amount with FFA and BF to calculate the fertilizer application amount.

The historical and future deposition data is taken from Lamarque et al. (2011). For crop specific N manure application data, we use M3 data for year 2000 and assume that it changes over the historcal and under two future scenarios at the same rates as the N fertilizer amount. Then we add spatial and time varying N fertilizer N manure, and N deposition amounts to estimate N input.

Text S4. Estimation of Irrigation Water Amount

The irrigation amount (W_{irrig}) is estimated as the soil moisture deficit between irrigation target (W_t) and soil water content (W_{liq}) within the root-zone as follows:

$$W_{irrg} = W_t - W_{liq} \tag{SE5}$$

where W_t is defined as soil moisture content without water stress (i.e., WS is 1.0) for crop photosynthesis during the growing period.

The irrigation scheme adds W_{irrig} directly to the topsoil layer, analogously to drip irrigation. The estimated W_{irrig} is withdrawn first from surface runoff and drainage. If surface runoff plus drainage is less than W_{irrig}, the remaining requirement of irrigation is extracted from river water storage (i.e., accumulated total runoff). To estimate these water we have incorporated a river transport module (RTM) into ISAM (Sharma et al, 2018). RTM is used to distribute total runoff from the land surface model to the downstream systems such as rivers and oceans. In RTM the water is routed from each grid cell to the neighboring grid cell by using a linear transport scheme (Oleson et al., 2013). However, the water demand for crops may still not be met with these sources in some dry seasons or areas, because the water resources and management, such as dynamic reservoir operations, are not accounted for in the model. This deficit of irrigation demand causes negative values of river water storages which should be met by water diversion from outside the rivers (Leng et al., 2015)(Leng et al., 2015). In this study we assume that the deficit of irrigation demand is met by the groundwater.

Irrigation is applied at each time step when the leaf area index (LAI) of the crop is greater than zero and root-zone soil water stress (WS) is less than 1.0 (i.e., water is limiting photosynthesis). The WS is expressed as an index ranging from 0 to 1in ISAM (Song et al., 2016). The closer WS is to 1, the lower the effect of water stress on crop photosynthesis. The model estimated annual applied irrigation water is evaluated with 11 global gridded crop models, which participated in AgMIP project (Müller et al. 2019). The simulation input data, including the weather data and N fertilizer inputs, were obtained from Müller et al. (2019). More details of the experimental setup and weather datasets can be found in Müller et al. (2019). We calculated the global irrigation water for ISAM by aggregating all grid cell values according to the fraction of irrigation areas, as described by MIRCA2000 (Portmann et al., 2010). Our model estimated irrigation demand due to growing maize and soybean on irrigated croplands are approximately 47.6 km^3/yr and 8.0 km^3/yr, which fall within AgMIP estimated range values (Figure S5).

Text S5. Estimation of Crop Specific Planting Time

The planting time ($DOY_{planting}$) (Defined as the Julian day of the year) for maize and soybean at each grid cell is estimated to be the later of that estimated from climate (temperature and precipitation) conditions ($DOY_{climate}$), and that estimated from phenological heat unit values (DOY_{phu}):

$$DOY_{planting} = \max (DOY_{climate}, DOY_{phu}) \quad \text{(SE6)}$$

For the calculation of $DOY_{climate}$ we assume that the planting time is dependent on inter-annual precipitation and temperature variability. For example, planting time in tropical regions, where distinct wet and dry periods exist, usually happens when the first rainy season of the year starts. In contrast, sowing processes in temperate regions start right after the winter season, as long as the temperature is sufficiently warm to avoid frostiness (Sacks et al., 2010). Since the planting time could vary with the season, we define different seasonality types for planting time, which are determined by calculating annual average variation coefficients (CV) for temperature and precipitation using monthly CRU-NCEP climate data for the period 1901-1950 (Waha et al., 2012). The CV is calculated for temperature (K) and precipitation (mm) respectively as follows:

$$\mathrm{CV} = \frac{\sum_{y=1}^{N} \mathrm{CV}_y}{N} \quad \text{(SE7a)}$$

$$\mathrm{CV}_y = \frac{\sigma_y}{\mu_y} \quad \text{(SE7b)}$$

where y is the year, CV_y is the variation coefficient of temperature or precipitation in year y, N is the number of years, σ_y is the standard deviation of temperature or precipitation in year y, and μ_y the annual mean temperature or precipitation in year y. The following equations are used to calculate σ_y and μ_y:

$$\sigma_y = \sqrt{\frac{1}{12-1} \times \sum_{m=1}^{12} \overline{Z_{m,y}} - \mu_y} \quad \text{(SE8)}$$

$$\mu_y = \frac{1}{12} \times \sum_{m=1}^{12} \overline{Z_{m,y}} \quad \text{(SE9)}$$

$$\overline{Z_{m,y}} = \alpha \times Z_{m,y} + (1-\alpha) \times \overline{Z_{m,y-1}} \quad \text{(SE8)}$$

where $Z_{m,y}$ is the mean temperature or precipitation of the month m in year y, $\overline{Z_{m,y}}$ is the exponential weighted moving average temperature or precipitation of a month m in year y, and α is the coefficient representing the degree of weighting (with a value of 0.05). For the first year of $Z_{m,y}$ (y=1), α is 1.0.

The seasonality types are determined based on the multi-year average of variation coefficients for temperature (CV_t) and precipitation (CV_p) and then classify into following four seasonality types:

(1) Temperature seasonality: $CV_t > 0.01$ and $CV_p <= 0.4$
(2) Precipitation seasonality: $CV_t <= 0.01$ and $CV_p > 0.4$
(3) No temperature and precipitation seasonality: $CV_t <= 0.01$ and $CV_p <= 0.4$
(4) Both temperature and precipitation seasonality: $CV_t > 0.01$ and $CV_p > 0.4$

For planting time decisions, we distribute each seasonality types into three planting conditions, temperature-limited (1), precipitation-limited (2), and non-climate-limited (3). In situations where both temperature and precipitation seasonality co-exist (4), we distinguish them by the difference in multi-year mean of daily minimum temperature (T_{min}). If T_{min} is equal to or below 283.16 K, the temperature is a determining factor for planting time. If T_{min} is higher than 283.16 K, precipitation is the determining factor, which uses the same algorithm of planting as precipitation-limited planting.

Maize and soybean must meet the following requirements for planting day.

$$\mathrm{DOY_{climate}} \geq \mathrm{DOY_{min}} \quad \text{(SE9)}$$

$$\mathrm{DOY_{climate}} \leq \mathrm{DOY_{max}} \quad \text{(SE10)}$$

$$\mathrm{T_{air7d}} > \mathrm{T_{base}} \quad \text{(SE11)}$$

$$\mathrm{T_{soil8d}} > \mathrm{T_{soil\_min}} \quad \text{(SE12)}$$

$$\mathrm{P_{d8}} > \mathrm{P_{min}} \quad \text{(SE13)}$$

$$\mathrm{P_{m\_avg}} > \mathrm{P_{m\_avg\_min}} \quad \text{(SE14)}$$

where $\mathrm{T_{air7d}}$ is the 7-day running mean of daily air temperature, $\mathrm{T_{soil8d}}$ 8-day running mean of daily root-zone average soil temperature, $\mathrm{P_{d8}}$ accumulated precipitation of the past eight consecutive days, and $\mathrm{P_{m\_avg}}$ 50-year average of monthly precipitation. Other crop-specific variables are defined in Table S1.

The second method to calculate the planting day (DOY_{phu}) assumes the day when the accumulated phenological heat unit (PHU_0) reaches a certain minimum threshold (β*PHU_{min}). PHU_0 is calculated by subtracting the threshold temperature of 273.16 K from the average daily air temperature (T_{air}) as follows.

$$\mathrm{PHU_0} = \mathrm{PHU_0} + \mathrm{T_{air}} - 273.16 \qquad \text{if } \mathrm{T_{air}} > 273.16\ \mathrm{K} \quad \text{(SE15)}$$

$$\mathrm{DOY_{phu}} = \mathrm{DOY} \qquad \text{if } \mathrm{PHU_0} \geq \mathrm{PHU_{min}} \times \beta \quad \text{(SE16)}$$

where PHU_{min} is the mean of annual PHU_0 for the period 1901-1950. β is the fractional parameter for maize (0.1) and soybean (0.12).

We evaluate simulated planting time with the data compiled by AgMIP (Elliott et al., 2015). This data is compiled using planting time data from two global crop calendars SAGE (Sacks et al., 2010) and MIRCA2000 (Portmann et al., 2010), as well as using a land surface model (LPJmL) driven data (Waha et al., 2012). The data availability and details can be found in Elliott et al. (2015).

Overall, the simulated spatial patterns of planting days for both crops match fairly well with the AgMIP data (Figure S6). For the regions NA, EU, and Northeastern CHN, which fall in the temperature-limited planting regions, the calculations for maize planting day appear to be similar to AgMIP data, whereas regions SA, SSEA, and AF, which fall in precipitation-limited and non-climate-limited regions, the estimated results are somewhat inconsistent with AgMIP data. For example, the main disagreements are shown for maize in countries like Thailand, Indonesia, Malaysia, Vietnam, and southeast CHN where simulated planting day is prior to AgMIP data. Our study findings are similar to the findings of previous studies (Deryng et al., 2011; Stehfest et al., 2007). This suggests that the algorithm for non-climate-limited planting is not well calibrated to reproduce planting time, which may not be determined based on the climatic conditions, but determined somewhat arbitrary. In regions of precipitation-limited planting, our estimation does not consider any effects of irrigation and soil moisture on planting time for maize, which may also make the difference in choice of planting time. Similar discrepancies are found for soybean. Simulated results are different in SSEA, SA, and Australia, which are in the precipitation-limited or non-climate-limited planting regions.

Text S6. Seeding and Plant Residue Removal Rates

The carbon stored in the seeds ($C_{storage}$) during the emergence period is determined based on the following equation (Song et al., 2013):

$$C_{storage} = C_{storage\_ref} \times \frac{R_{seed}}{R_{seed\_ref}} \quad \text{(SE17)}$$

where R_{seed}: seeding rate; R_{seed_ref}: reference seeding rate; and $C_{storage\_ref}$: referenced carbon storage in seed.

In the previous version of ISAM, R_{seed}, R_{seed_ref}, and R_{seed_ref} kept constant at each grid cell according to the collected data in the United States (US) for maize and soybean (Table S2) (Song et al., 2013; 2016). We now assume varying values for R_{seed} and $C_{storage\_ref}$ in ISAM based on the literature as changing seeding rate is found to influence the soybean yield (De Bruin & Pedersen, 2008),.

In the temperate regions with higer seasonal temperature variations, such as EU, NA, and CHN, (Text S5), we use the values for sybean based on Song et al. (2013) (Table S2). For other regions, such as areas in AF and SSEA, we use the seeding rate and initial carbon storage in seed as referenced seeding rate from a farmers' guide based on Dugje et al., (2009) (Table S2). For maize, the seeding rates are assumed to be the same for all regions based on Song et al. (2013).

Similar to the difference in planting processes, the removal of residue (in %) at the harvest time is chosen from the previous studies in Africa and the US. In Sub-Saharan Africa 85% of above-ground crop residues are assumed to be removed at the harvest time (Doraiswamy et al., 2007; Folberth et al., 2012). In contrast, about 30% of the crop residues are recycled in North America (Liu et al., 2010; Drewniak et al., 2015). For eaxmple, 30% of residue is removed in the US (Drewniak et al., 2015). Therefore, we assume residue removal of 30% for grids showing the temperature seasonality (Text S5) and 85% for other grid cells. The rest of the residue is assumed to return to the soil surface (e.g., Kucharik & Brye, 2003; Verma et al., 2005)

Text S7. ISAM Model Simulations Yields for Maize and Soybean for FACE Sites

Two FACE sites data, which we used in this study to evaluate the model performance, conducted experiments in fully open-air, field conditions with increase in atmospheric CO_2 concentration ([CO_2]) from baseline (around 380 ppm) to 550 ppm. Table S3 summarizes two FACE site locations and elevated atmospheric CO_2 concentration.

Soybean FACE site (SoyFACE) in Illinois, the US is the first FACE study of soybean (Morgan et al., 2005). SoyFACE performs ambient and elevated CO_2 treatments for 2002–2011. The [CO_2] for the ambient case varies between 370 and 392 ppm for this period (hereafter referred to as ambient) and for the elevated case [CO_2] was set to 550 ppm for 2002-2008 and 585 ppm for 2009-2011 (hereafter referred to as elevated) according to the filed treatment (Gray et al., 2016). Maize was grown over two years (2007-2008) at FACE site in Germany. The circular main plot was spitted into a well-watered (WET) and a dry (DRY) semicircular subplot (Manderscheid et al., 2014). The WET conditions keep sufficient water supply under ambient [CO_2] (378 ppm) and elevated [CO_2] (550 ppm) concentrations. The model is run with site-specific planting and harvest times, seeding density, actual period of [CO_2] enrichment and irrigation, and amounts of N fertilizer and irrigation. We only compare the modeled irrigated yield with WET FACE condition, because the sufficient information was not provided in the literature for the DRY FACE condition (Deryng et al., 2016).

For the simulation for these sites, the model was first spun-up using climate forcing and input for soil variables. Next, the model was run for two cases. The first was the ambient [CO_2] case, and the second was elevated [CO_2] case.

For the SoyFACE site simulations we use half-hourly time step climate forcing data compiled from the Bondville, IL site, which is the nearest Surface Radiation Network (SURFRAD) station (40.05°N, 88.37°W) and Willard airport (40.04°N, 88.27°W) site. We used precipitation data from the Willard airport and other meteorological data from SURFRAD site (Vanloocke et al., 2010). The missing data for SURFRAD site was filled with the data collected at Willard Airport. For German FACE site runs we use hourly time step climate forcing data of CRU-NCEP for the period 2007-2008. For each face site we prescribe layer-specific soil dataset, for example, the sand/clay fraction, organic matter, bulk density, and other hydraulic parameters. These parameter values for SoyFACE site are taken from the soil survey geographic database (SSURGO) database (USDA, 2019) and for German FACE site from the Global Soil Dataset for use in Earth System Models (GSDE, Shangguan et al., 2014).

The evaluation of ISAM results with FACE sites show that the original version of ISAM (ISAM_O) estimated effects of [CO_2] enrichment on crop yields for maize was consistent with FACE site data, but overestimated for soybean for elevated [CO_2] case (Figure S7a), because, the electron transport rate (J) calculation used the linear function of the light response curve (Chen et al., 2011):

$$J = \varepsilon \alpha \o \qquad \text{(SE18)}$$

where ε is 0.04 mol mol^{-1} for maize (Arora, 2003); and 0.08 for Soybean (Sellers et al., 1996) is quantum yield of electron transport, α (=4.6 μmol J^{-1}) is conversion from photosynthetically active radiation to photosynthetic photon flux, and ø (W m^{-2}) is absorbed photosynthetically active radiation, which is calculated from solar fluxes using the two-stream approximation and varies between sunlit and shaded leaves for photosynthesis (Song et al., 2013).

To address this issue, we added curvature to the light response curve in *J* for the revised version of the ISAM (ISAM_R) (Bonan et al., 2011):

$$J = \min(\varepsilon \alpha ø, J_{max}/4) \quad \text{(SE19)}$$

where J_{max} is maximum potential electron transport rate (Bonan et al., 2011; Song et al., 2013).

After implementation of curvature to the light response curve, ISAM_R estimated results were consistent with the measured values (Figure S7a). For example, ISAM_R estimated yields for the average ambient and elevated measured yields were 353 ± 40 g/m^2 and 416 ± 40 g/m^2 compared to the measured values of 382 ± 38 g/m^2 and 425 ± 44 g/m^2 over the 5-year (2002, 2004-2007) growing season (Twine et al., 2013).

The simulated canopy temperature and stomatal conductance are also evaluated with measured data in years 2004-2011 (Figures S7b and S7c). Our results indicated that after revised photosynthetic pathway calculated by ISAM_R is also able to reduce the biases in the simulated magnitudes of stomatal conductance under ambient and elevated [CO_2]. The modeled stomatal conductance was decreased by 21%, and observation show a 30% average decrease due to CO_2 fertilization effect. In addition, canopy temperature increased because of decrease in stomatal conductance under elevated [CO_2]. ISAM_R estimated average canopy temperature increased by 0.28K (1.1%), which was similar to observed values of around 0.21K (0.9%) (Figure S7b).

Text S8. Implementation of the N Stress Effect on Carbon Allocation

We evaluate ISAM estimated maize yield response to different application rates of N fertilizer with published results from six different site-level field experiments (Table S5). Our modeling analysis suggests that the biases in the original version of ISAM (ISAM_O) estimated maize yield is large for the lower N input cases (Figure S8a) because the model underestimates the effect of N stresses (i.e., ratio of N supply and N demand) on grain formation and carbon allocation.

The field experiment studies suggest that the maize growth slows down at the lower N supply rates, causing decline in maize yield (Alemayehu et al., 2015; Gehl et al., 2005; Getachew & Belete, 2013; Hammad et al., 2011) and harvest index (ratio of harvested grain to aboveground biomass) (Akinnifesi et al., 2007; Attia et al., 2015; Kucharik & Brye, 2003; Nangia et al., 2008; Puntel et al., 2016). However, the model is overestimating the maize yields and harvest index at the lower N application rates, because the model overestimates the amount of carbon allocated to the grain formation under the N stress (i.e., ratio of N supply and N demand). However, model results for soybean are consistent with the measured data (Figure S8b). To overcome this deficiency, we implement in the model with N stress effect on carbon allocated to grain during initial and post-reproductive (grain-filling) periods (hereafter this version of the model is called ISAM_R). Therefore, at a lower N fertilizer rate, ISAM_R shows a stronger N stress, lower carbon allocation to grain formation and harvest index compared to ISAM_O case (Figure S8a).

We validate the modeled maize yield with site-specific observed values. Overall, ISAM_R estimated maize yields for different N fertilizer rates are compared well with the observation data (Figure S8a).

Text S9. Heat Stress effect on Crop Productivity

The model calculates the impact of heat stress on reduction in the carbon allocation amount to grain during the reproductive stage of the phenology as follows:

$$A_g = A_{g\_max} * HS \qquad \text{(SE20)}$$

where A_g is the updated and maximum carbon allocated fraction of net assimilated carbon to the grain pool during the reproductive stage of the phenology, A_{g_max} is an initial calibrated parameter without heat stress impact (Song et al., 2013), and HS is heat stress factor calculated based on Challinor et al. (2005) and has also been used in other studies (e.g., Deryng et al., 2014; Moriondo et al., 2011; Teixeira et al., 2013):

$$HS = \frac{1}{24}\sum_{i=1}^{24}\begin{cases} 1.0 & T_{mean\_i} \le T_{crit} \\ \frac{T_{limit} - T_{mean\_i}}{T_{limit} - T_{crit}} & T_{crit} < T_{mean\_i} < T_{limit} \\ 0.0 & T_{mean\_i} \ge T_{limit} \end{cases} \qquad \text{(SE21)}$$

where T_{limit} is limiting temperature at which full heat stress reaches, T_{mean_i} is hourly canopy temperature during the initial and reproductive or flowering stages of the phenology, and T_{crit} the critical temperature at which heat stress starts. For the temperature input in HS, we use crop canopy temperature calculated based on ISAM as the average between the temperatures of the sunlit and shaded leaf weighted by the fraction of sunlit and shaded leaf areas.

T_{crit} and T_{limit} vary among crop types taken in consideration current literature (Deryng et al., 2014; Teixeira et al., 2013). Here, T_{crit} for mize and soybean are 32°C and 35°C, whereas T_{limit} are 45°C and 40°C.

Text S10. The Calculation of the Percent Bias (PBIAS)

The PBIAS is calculated to compare modeled yield with measured yield at regional and global scales:

$$PBIAS = \frac{\sum_{i=1}^{M}\sum_{j=1}^{N}\left(Y_{i,j}^{o} - Y_{i,j}^{m}\right)}{\sum_{i=1}^{M}\sum_{j=1}^{N} Y_{i,j}^{o}} \times 100\% \qquad \text{(SE22)}$$

where $Y_{i,j}^{o}$ and $Y_{i,j}^{m}$ are the observed and modeled yearly yields for the available data *i* in the year *j*. M is the number of available data points. N is the number of years for each available data.

The positive PBIAS means the model yield is consistently underestimated compared to the observed yield. The closer the value of PBIAS to zero means the higher the accuracy of the model results (Song et al., 2015).

Text S11. Calculation of Detrended Yield

Following the method of Müller et al. (2017), we first aggregate ISAM estimated yields to regional values using equation (SE4). For the consistent purpose, ISAM follow the region definition of FAOstat (2017). We then calculate 5-year moving average (t-2 to t+2) yields based on ISAM and FAOstat over the period 1981-2007 and 3-year moving (t-1 to t+1) average yields at the boundary of this time period to get the yield trends at a regional and global scales. We eliminate the trend from ISAM model results and FAOstat data by subtracting the trended yield from actual yield. Note that no de-trended yields appear at boundary years, 1981 and 2007. So, de-trended yield shown in Figure S9 cover the period 1982-2006.

Text S12. CLM and AgMIP Model Results for the FACE Sites

To assess the performance models against FACE site data in Table S4, AgMIP project selected corresponding yield from the 6 AgMIP model simulations for climate change (CC) w/ CO_2 and CC w/o CO_2 at the grid cells matching the coordinates of FACE observations (Deryng et al., 2016). But temperatures are held constant for the AgMIP models experiment results reported in Table S6. Ambient [CO_2] in the FACE experiments varied between 360 and 380 ppm and elevated [CO_2] corresponds to 550 ppm. So, AgMIP used 10-year average estimates around the year 2050, which corresponds to the same increment of [CO_2] level rise relative to the baseline (550 ppm in 2050 to 380 ppm in 2000, respectively). We use the same method to extract yields from the CLM outputs of Ren et al. (2018). Given these limitation, the comparison of AgMIP and CLM model results with FACE sites should not be considered as a direct comparison. However, the comparisons can still demonstrate the difference between observed yield changes and simulated values from global crop models

Supplementary Tables

Table S1. Parameters of planting day for maize and soybean.

Definition (Symbol)	Climate-limited regions	Maize	Soybean
Minimum planting day (DOY_{min})*	Precipitation-limited	120 (270)	160 (314)
	Temperature-limited	80 (296)	100 (314)
	Non-climate limited	115 (115)	115 (314)
Maximum planting day (DOY_{max})*		166 (346)	181 (361)
Base temperature for crop planting and growth (T_{base}, K)		283.16	281.16
Critical soil temperature for planting (T_{soil_min}, K)	Precipitation-limited	285.2	285.2
	Temperature-limited	285.16	283.16
	Non-climate limited	0	0
Minimum accumulated 8-day precipitation for planting (P_{min}, mm)	Precipitation-limited	1	1
	Temperature-limited	0	0
	Non-climate limited	0	0
Annual average monthly precipitation requirement ($P_{m\_avg\_min}$, mm)	Precipitation-limited	60	60
	Temperature-limited	0	0
	Non-climate limited	0	0

*The maximum and minimum planting days are in the Northern Hemisphere, the corresponding days in the Southern Hemisphere are shown in brackets.

Table S2. The initial carbon storage in seed as referenced ($C_{storage\_ref}$), reference seeding rates (R_{seed_ref}), and seeding rates (R_{seed}) for maize and soybean by climate-limited regions*.

Crop type	Climate-limited planting regions	Reference Carbon Storage in Seed (gC/m^2)	Referenced seeding rate (seeds/acre)	Seeding rate (seeds/acre)	Reference
Maize	Precipitation-limited Temperature-limited Non-climate limited	20	62236	35000	Song et al. (2013; 2016)
Soybean	Temperature-limited	30	370644	370000	
	Precipitation-limited Non-climate limited	5	370644	179860	Dugje et al. (2009)

*See Supplementary Text S6

Table S3. Summary of two FACE sites.

Crop	Site location	Latitude (deg.)	Longitude (deg.)	Ambient CO_2 (ppm)	Elevated CO_2 (ppm)	Reference
Maize	Braunschweig, Germany	52.30	10.43	378	550	Manderscheid et al. (2014)
Soybean	Illinois, USA	40.05	-88.20	370-392	550, 585	Bernacchi et al. (2006); Gray et al. (2016); Morgan et al. (2005)

Table S4. ISAM estimated change (%) in maize and soybean yields due to elevated [CO_2] concentration are compared with FACE site data and CLM and AgMIP model results under wet/irrigated conditions[1].

Crop	FACE	Model		
		ISAM[4]	CLM[7]	AgMIP[7]
Maize	-1.0[2]	0.2	0.9	0.2 - 7.7
Soybean	14.4 ± 12.5[3]	17.5± 2.7[5] (32.1± 4.3)[6]	22	5.2 - 44.4

[1] The positive values are net sink of C by the terrestrial ecosystem
[2] German- FACE site
[3] SoyFACE site
[4] See supplementary Text S7 for ISAM simulations
[5] Calculated by the revised version of ISAM
[6] Calculated by the original version of ISAM
[7] Deryng et al. (2016) (See Text S11 for CLM and AgMIP models simulations)

Table S5. Information for various sites, which are used to evaluate the model response to different level of N fertilizer applicate rates.

Site	Location	Lat. (deg)	Long. (deg)	N fertilizer (kgN/ha/yr)	Year	Soil	Reference
Maize							
Wisconsin's Agricultural Research Station (WARS)	Arlington, WI, USA	43.28° N	89.37° W	0, 180	1995-2000	silt loam	Kucharik & Brye (2003)
Agricultural Engineering & Agronomy Research Farm (AEARF)	Ames, IA, USA	42.01° N	93.79° W	0, 67, 134, 201, 268	1999-2014	loam	Puntel et al. (2016)
University of Tennessee Milan Research and Education Center (UTMREU)	Milan, TN, USA	35.93° N	88.72° W	0, 61.6, 123.2, 184.8, 246.4	2007-2011	silt loam	Boyer et al. (2013)
Florence	Florence, SC, USA	34.24° N	79.81° W	68, 101, 135, 169	1999-2001	loam sand	Stone et al., (2010)
Oakes	Oakes, ND, USA	46.07° N	98.10° W	0, 45, 90, 135, 180, 225	1990-1995	loam sand	Derby et al. (2005)
Brunswick	Brunswick, NE, USA	42.33° N	79.92° W	0, 56, 112, 168, 224, 280	2006-2008	loam sand	Attia et al. (2015)
Soybean							
University of Nebraska Field Laboratory at Mead	Mead, NE	41.169 °N	96.466° W	0, 56, 112	1974, 1976	Silty clay loam	Al-Ithawi et al. (1980)

Table S6. Maize and soybean yields (t/ha) at global and regional scales averaged over the period 1996-2005 for the reference case (E_{Ref}) and for the [CO_2] (E_{CO2}), climate (E_{Cli}), irrigation (E_{Irr}), nitrogen input (E_{Nit}) and harvest areas (E_{Har}) factor cases; and the % contribution of individual factor to the Reference case yield over the average period 1996-2005*. The lowest two panels show the the contribution of individual factor change (%) to the yield change from 1996-2005 to 2090s under RCP4.5 and RCP 8.5 scenarios**.

Global/Region	Reference		[CO_2]		Climate		N input		Irrigation		Harvest Area	
	Maize	Soy	Maize	Soy	Maize	Soy	Maize	Soy	Maize	Soy	Maize	Soy
Average crop yield over the period 1996-2005, t/ha												
Global	4.52	2.12	4.32	1.77	4.41	2.03	2.92	1.97	4.20	2.07		
North America (NA)	7.86	2.68	7.48	2.37	7.48	2.56	5.27	2.59	7.31	2.62		
South America (SA)	3.25	1.75	3.16	1.38	3.28	1.69	2.23	1.62	3.20	1.75		
Europe (EU)	5.78	2.56	5.46	2.25	5.62	2.44	3.74	2.50	5.35	2.26		
Africa (AF)	1.93	0.97	1.82	0.69	1.95	1.06	1.61	0.90	1.82	0.90		
China (CHN)	5.40	2.40	5.21	1.96	5.47	2.32	2.71	2.07	4.69	2.27		
South and South East Asia (SSEA)	1.91	0.89	1.85	0.56	1.88	0.86	1.15	0.60	1.86	0.88		
Contribution of individual factor (%) to the reference case over the period 1996-2005*												
Global			4.38	16.40	2.27	3.92	35.37	7.08	7.05	2.09		
North America (NA)			4.86	11.31	4.79	4.19	33.01	3.14	7.02	2.15		
South America (SA)			2.88	21.60	-0.91	3.55	31.49	7.53	1.65	0.15		
Europe (EU)			5.56	12.26	2.77	4.61	35.33	2.40	7.39	11.95		
Africa (AF)			5.71	28.32	-0.78	-9.74	16.96	7.14	5.80	6.65		
China (CHN)			3.56	18.33	-1.32	3.32	49.80	13.95	13.14	5.71		
South and South East Asia (SSEA)			2.76	36.99	1.52	2.86	39.83	32.21	2.37	0.67		
Contribution of individual factor to the yield change from 1996-2005 and 2090s under RCP4.5 (%)**												
Global	1.00	15.44	7.04	27.90	-6.59	-4.31	53.46	15.19	3.46	1.82	-19.75	-7.16
North America (NA)	7.79	12.94	7.94	20.29	-2.89	-3.95	53.03	2.91	5.63	1.93	-3.60	-1.48
South America (SA)	51.84	35.41	8.69	34.64	-14.37	-2.04	87.26	22.90	1.53	0.36	0.80	-5.59
Europe (EU)	11.73	-4.25	13.98	19.25	-12.03	-17.41	56.82	2.69	3.49	9.76	-6.28	-9.22
Africa (AF)	35.51	27.30	8.38	42.98	-6.15	-24.39	64.60	28.31	2.06	4.63	-22.64	-6.42
China (CHN)	-6.81	10.13	5.63	27.72	-4.22	-10.73	51.92	20.37	8.07	4.96	-6.91	-1.33
South and South East Asia (SSEA)	41.94	56.48	6.70	67.24	-9.44	-18.83	83.35	40.49	6.17	12.46	8.86	17.54
Contribution of individual factor to the yield change (%) from 1996-2005 and 2090s under RCP8.5 (%)**												
Global	-22.05	13.95	9.64	46.50	-11.03	-30.15	31.51	9.34	2.83	2.19	-13.28	-4.24
North America (NA)	-10.53	13.50	9.53	33.20	-14.63	-26.12	41.59	2.05	2.70	1.06	-0.82	0.44
South America (SA)	-8.82	28.02	8.09	58.23	-6.30	-33.41	33.79	11.71	1.75	1.36	8.89	1.75
Europe (EU)	4.36	4.18	27.08	43.10	-14.68	-38.62	44.98	2.38	5.61	23.73	-2.13	2.37
Africa (AF)	5.53	49.17	9.23	77.42	-9.70	-44.13	31.31	18.90	1.30	6.35	0.01	2.57

China (CHN)	-19.60	8.97	12.66	47.67	-25.20	-37.18	37.38	17.73	7.42	4.72	-2.82	-0.21
South and South East Asia (SSEA)	-11.63	65.73	5.63	105.09	-4.73	-56.07	36.76	39.88	3.03	12.76	1.74	9.72

*(E_{Ref} in 1996-2005 - E_{XXX} in 1996-2005)/E_{Ref} in 1996-2005. E_{XXX} represents E_{CO2}, E_{Cli}, E_{Irr}, E_{Nit} or E_{Har}

**(E_{Ref} in 2090s - E_{XXX} in 2090s)/E_{Ref} in 1996-2005. E_{XXX} represents E_{CO2}, E_{Cli}, E_{Irr}, E_{Nit} or E_{Har}

Supplementary Figure Captions

Figure S1. Regional distributions map. The acronym for each region is in parentheses.

Figure S2. Global total (a) harvested areas (Million ha) and (b) nitrogen input amount (deposition, manure, and fertilizer) (trillion gram N) for maize and soybean from 1950 to 2100. The harvested areas and N input amount for the historical time period are calculated using the method described in Supplementary Text S2 and Text S3. The result for the period 2016-2100 are based on RCP 4.5 and RCP 8.5 scenarios.

Figure S3. Harvested area fraction plotted at 0.5º x 0.5º grid resolution for maize (left panel) and soybean (right panel) for 1996-2005 (top row) and 2090s (2090-2099) under RCP4.5 (middle row) and RCP8.5 (bottom row).

Figure S4. Nitrogen input rate (kgN/ha for 0.5º x 0.5° grid) for maize (left panel) and soybean (right panel) for 1996-2005 (top row), and 2090s (2090-2099) under RCP4.5 (middle row) and RCP8.5 (bottom row).

Figure S5. Comparison of ISAM estimated global total irrigated water for (a) maize and (b) soybean with AgMIP models (Müller et al., 2019) for the period 1905-2012. The green solid line shows the AgMIP ensemble median values and the shaded area shows the interquartile range.

Figure S6. Comparison of ISAM estimated spatial distributions of maize and soybean planting days (Julian day of the year) averaged for year 1996-2005 with AgMIP data (Elliott et al., 2015).

Figure S7. Comparison of measured (red bars) and modeled (orginal version represented by ISAM_O (dark gray bars), and revise version by ISAM_R (bright gray bars) at the SoyFACE for (a) ratio of yield in elevated to ambient [CO_2] for the year 2002, and 2004-2008, (b) change in canopy temperature in elevated relative to ambient CO_2 during daylightwhen photosynthetically active radiation is > 50 μmol/m^2/s for 2004-2011, and (c) midday stomatal conductance under ambient and elevated CO_2 for 2004-2011. The error bar in (a) shows one standard deviation of observed yield with 7 different cultivars and in (b) and (c) are means ± standard errors of temporal variability.

Figure S8a. Measured and simulated yields of maize with different N fertilizer levels at (a) WARS, (b) AEARF, (c) UTMREU, (d) Florence, (e) Oakes, and (f) Brunswick sites (Table S3). The red solid dots show measured values, green solid triangles show simulated results with original version of ISAM (ISAM_O), and blue solid diamonds for revised version of ISAM (ISAM_R). Bars show ± standard deviation indicating the temporal variability in measured yields of maize.

Figure S8b. Same as Figure S8a, but for soybean with different N fertilizer levels at University of Nebraska Field Laboratory, Mead site.

Figure S9. Comparision of ISAM estimated detrending maize (left panel), and soybean (right panel) yields (t/ha) for regional and global scale for the the period 1982-2006 with FAOstat data set. The "*r*" value in each figure is the correlation coefficient.

Figure S10. Maize (left panel) and soybean (right panel) changes in yields (%) for the 2090s relative to the 1996-2005 under RCP4.5 (top row) and RCP 8.5 scenarios (bottom row). Results are plotted at 0.5^{o} x 0.5^{o} degree spatial resolution.

Figure S11a. Maize and soybean yield changes (%) averaged for 1996-2005 due to effects of CO_2, climate, irrigation and nitrogen inputfactors. Simulated areas are masked by crop-specific harvested areas averaged for 1996-2005.

Figure S11b. Same as Figure S12a, but the changes (%) from 1996-2005 and to 2090s under RCP4.5.

Figure S11c. Same as Figure S11a, but the changes (%) from 1996-2005 and to 2090s under RCP8.5.

Figure S12. Peak leaf area index (LAI) for maize and soybean averged for 1996-2005 and 2090 under RCP 4.5 and RCP8.5 scenarios.

Figure S13 Simulated leaf net photosynthetic rates for C4 crops, maize and C3 crops, soybean response to leaf temperature. Solid line is maize and dashed line is soybean.

Figure S14. Maps of effect of heat stress on maize and soybean yield (%) for RCP4.5 and RCP8.5 in the 2090s. Values show (yield w/ heat stress minus yield w/o heat stress) / (yield w/o heat stress) *100%.

Figure S15. Changes in harvested areas (solid bars) and production (hatched bars) for (a) maize and (b) soybean under RCP4.5 and RCP8.5 scenarios (red bars) by the 2090s relative to the period of mean 1996-2005.

Supplementary Figures

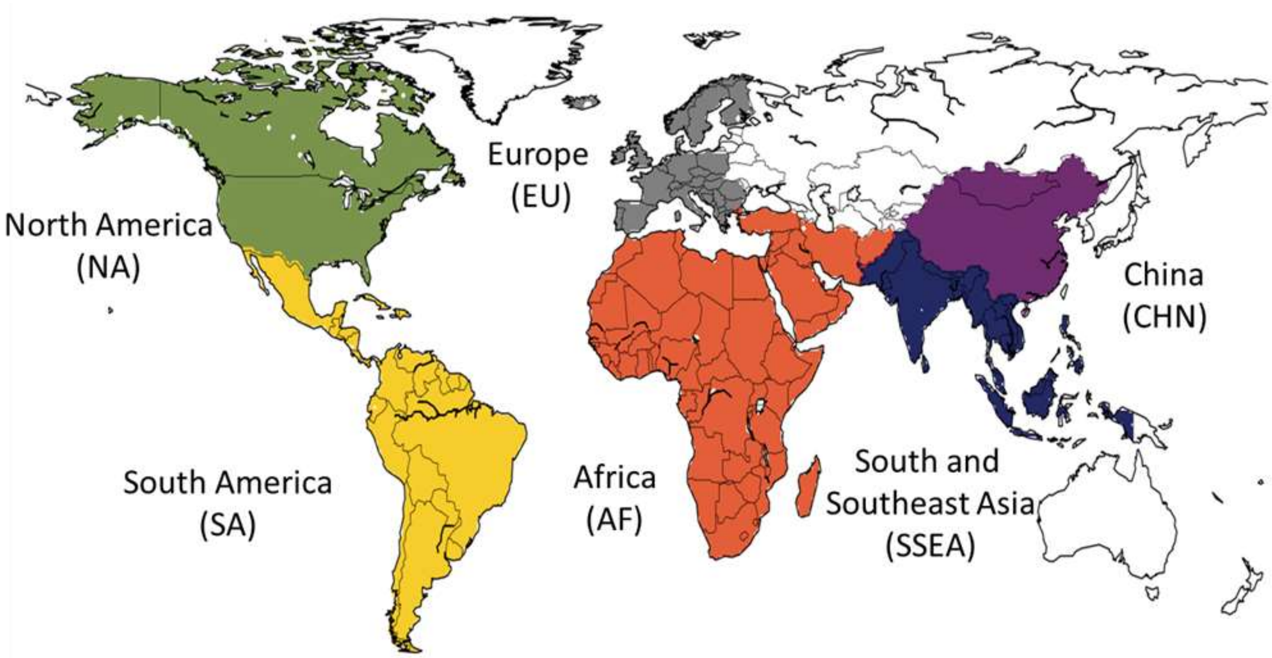

Figure S1. Regional distributions map. The acronym for each region is in parentheses.

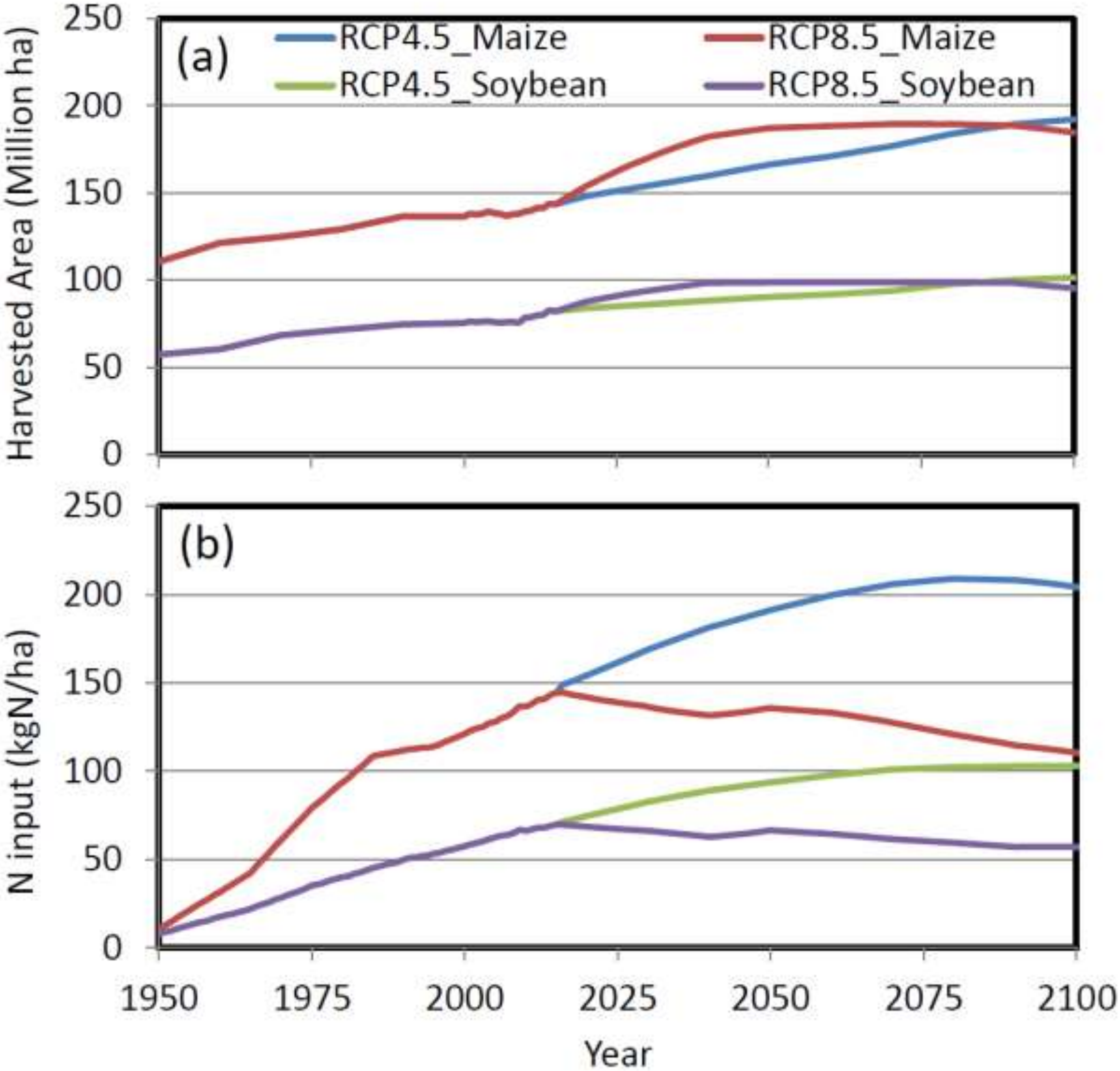

Figure S2. Global total (a) harvested areas (Million ha) and (b) nitrogen input amount (deposition, manure, and fertilizer) (kgN/ha) for maize and soybean from 1950 to 2100. The harvested areas and N input amount for the historical time period are calculated using the method described in Supplementary Text S2 and Text S3. The result for the period 2016-2100 are based on RCP 4.5 and RCP 8.5 scenarios.

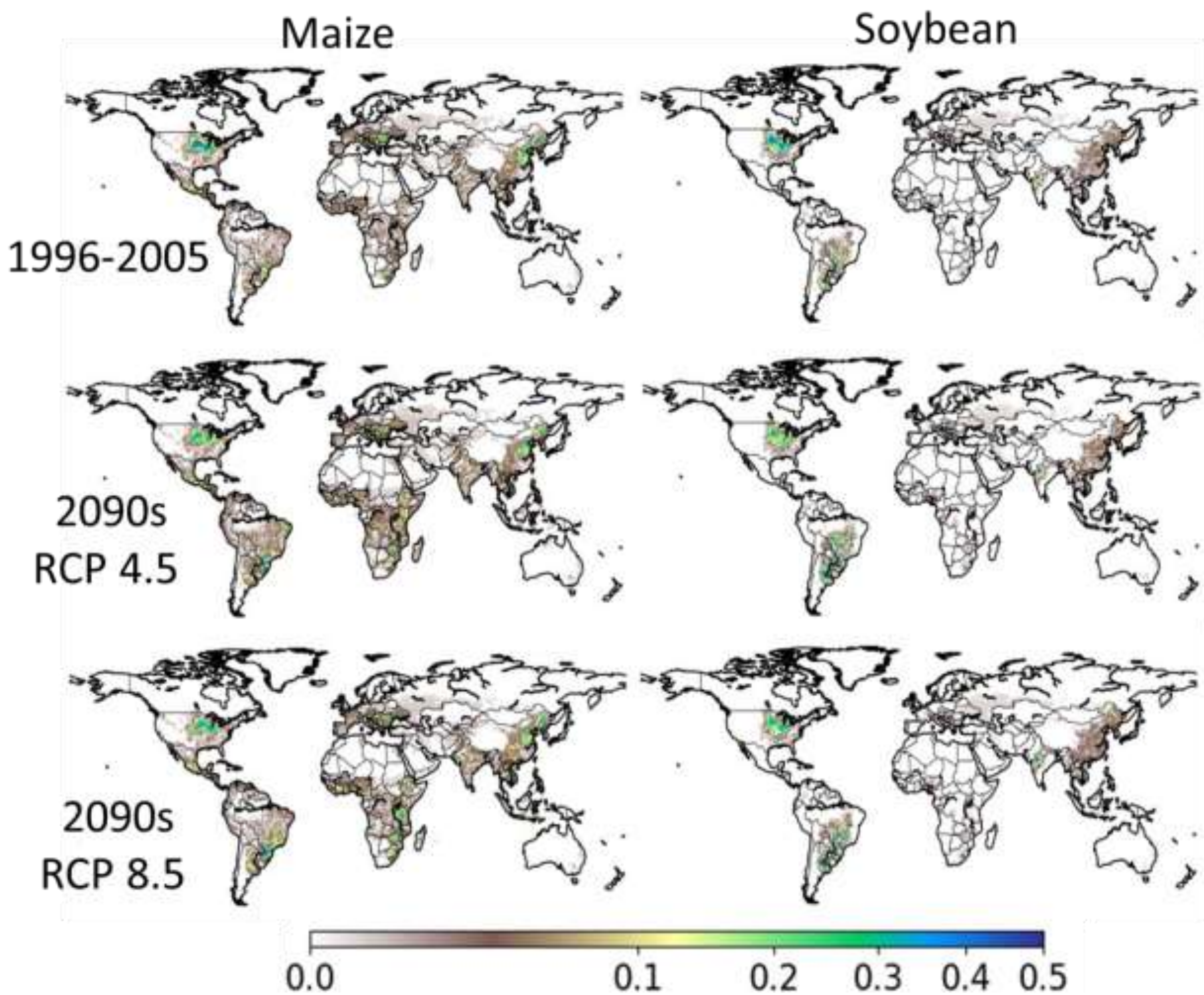

Figure S3. Harvested area fraction plotted at 0.5^o x 0.5^o grid resolution for maize (left panel) and soybean (right panel) for 1996-2005 (top row) and 2090s (2090-2099) under RCP4.5 (middle row) and RCP8.5 (bottom row).

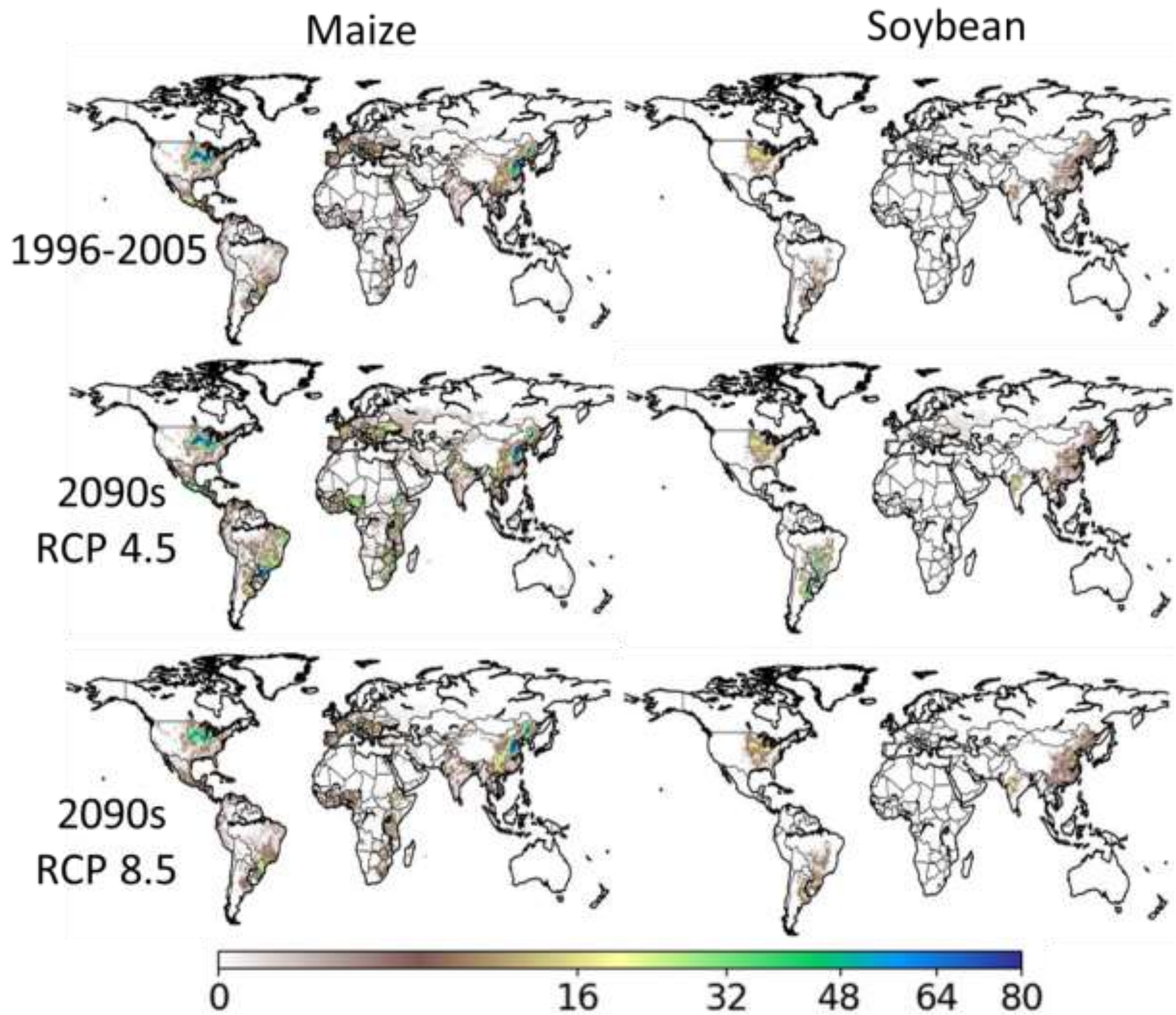

Figure S4. Nitrogen input rate (kgN/ha for 0.5º x 0.5° grid) for maize (left panel) and soybean (right panel) for 1996-2005 (top row), and 2090s (2090-2099) under RCP4.5 (middle row) and RCP8.5 (bottom row).

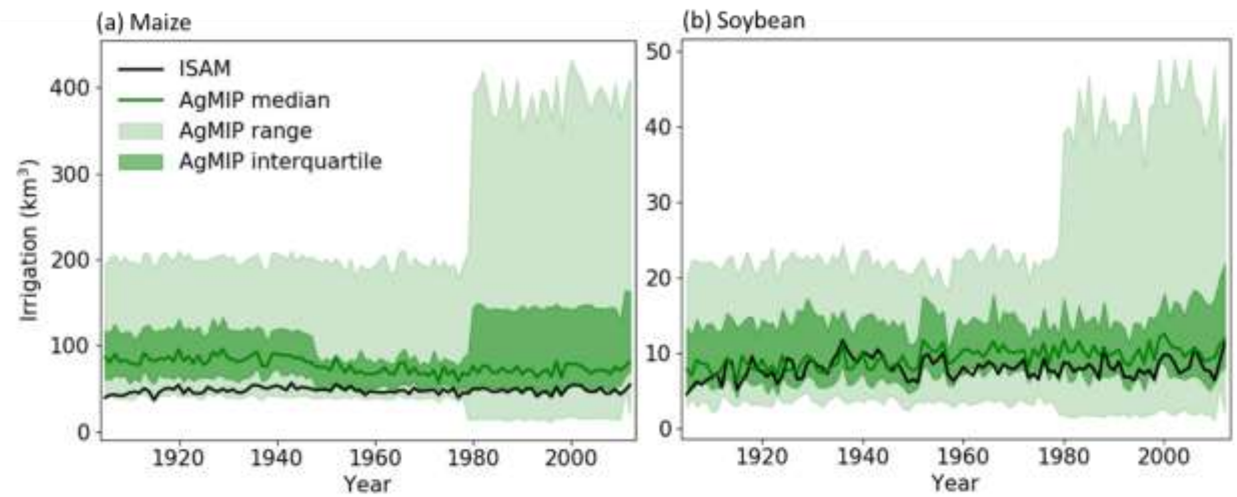

Figure S5. Comparison of ISAM estimated global total irrigated water for (a) maize and (b) soybean with AgMIP models (Müller et al., 2019) for the period 1905-2012. The green solid line shows the AgMIP ensemble median values and the shaded area shows the interquartile range.

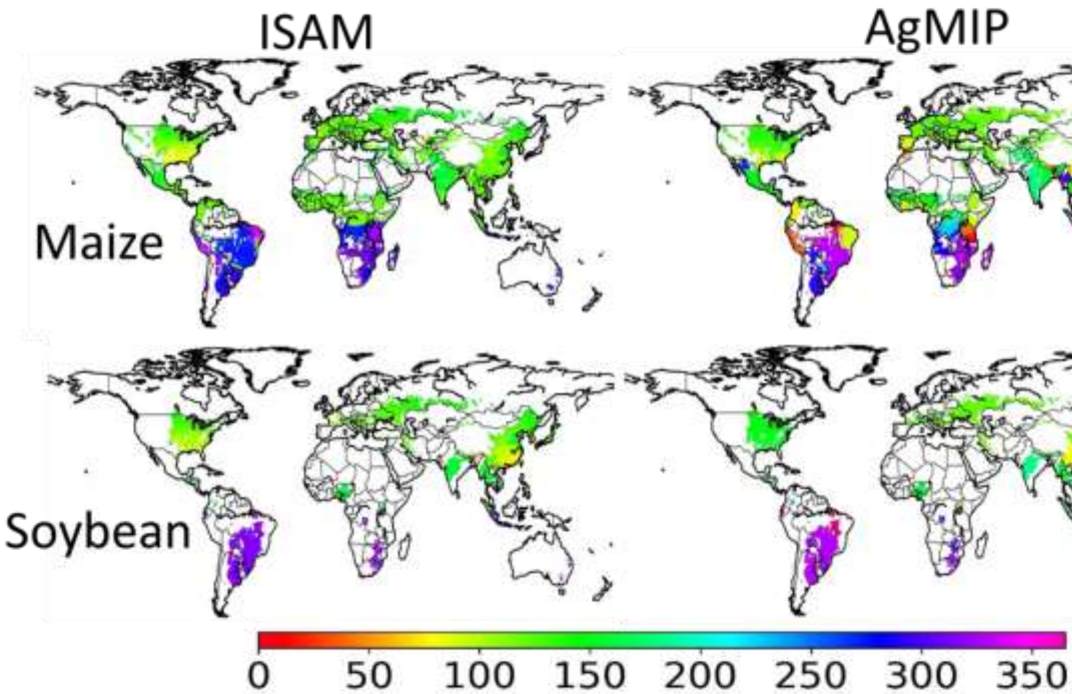

Figure S6. Comparison of ISAM estimated spatial distributions of maize and soybean planting days (Julian day of the year) averaged for year 1996-2005 with AgMIP data (Elliott et al., 2015).

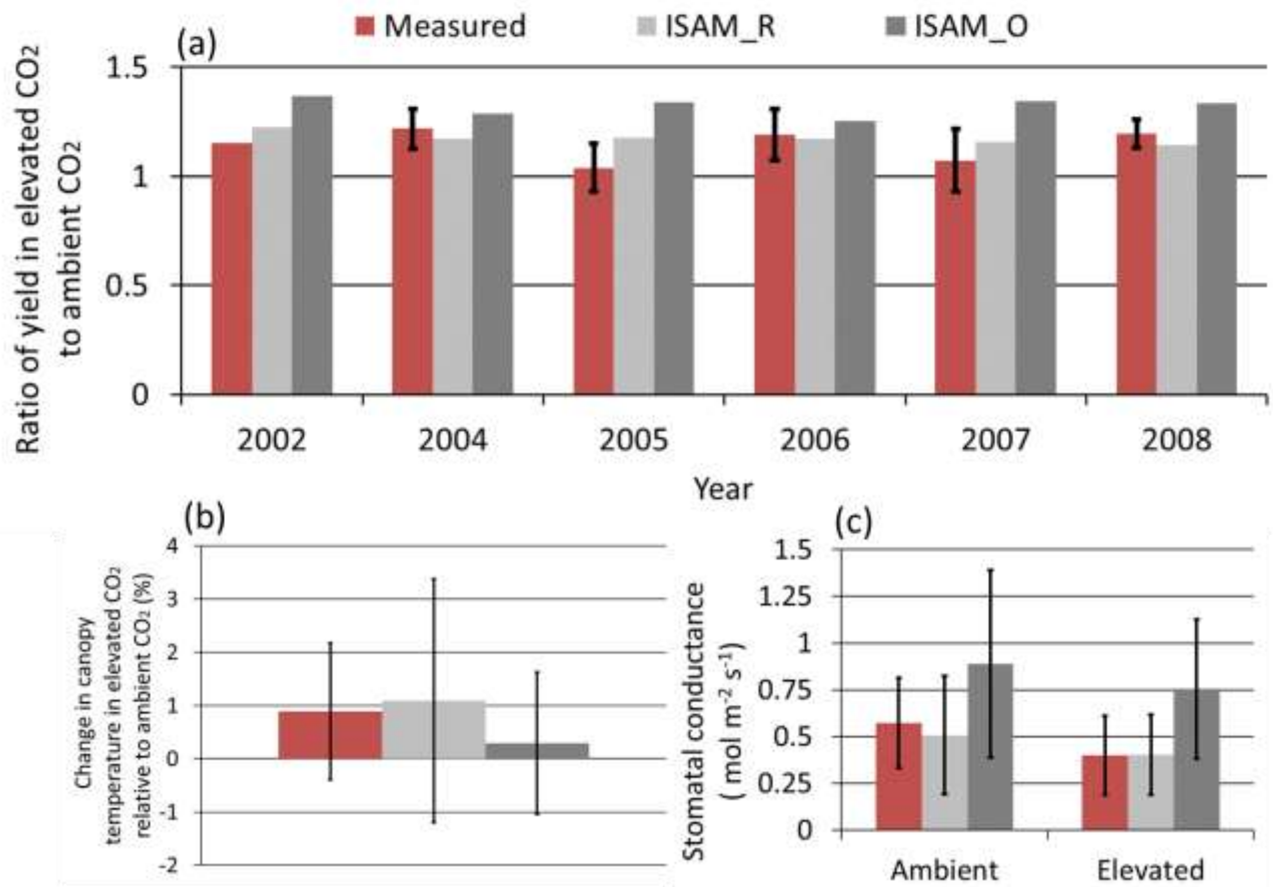

Figure S7. Comparison of measured (red bars) and modeled (orginal version represented by ISAM_O (dark gray bars), and revise version by ISAM_R (bright gray bars) at the SoyFACE for (a) ratio of yield in elevated to ambient [CO_2] for the year 2002, and 2004-2008, (b) change in canopy temperature in elevated relative to ambient CO_2 during daylightwhen photosynthetically active radiation is > 50 μmol/m^2/s for 2004-2011, and (c) midday stomatal conductance under ambient and elevated CO_2 for 2004-2011. The error bar in (a) shows one standard deviation of observed yield with 7 different cultivars and in (b) and (c) are means ± standard errors of temporal variability.

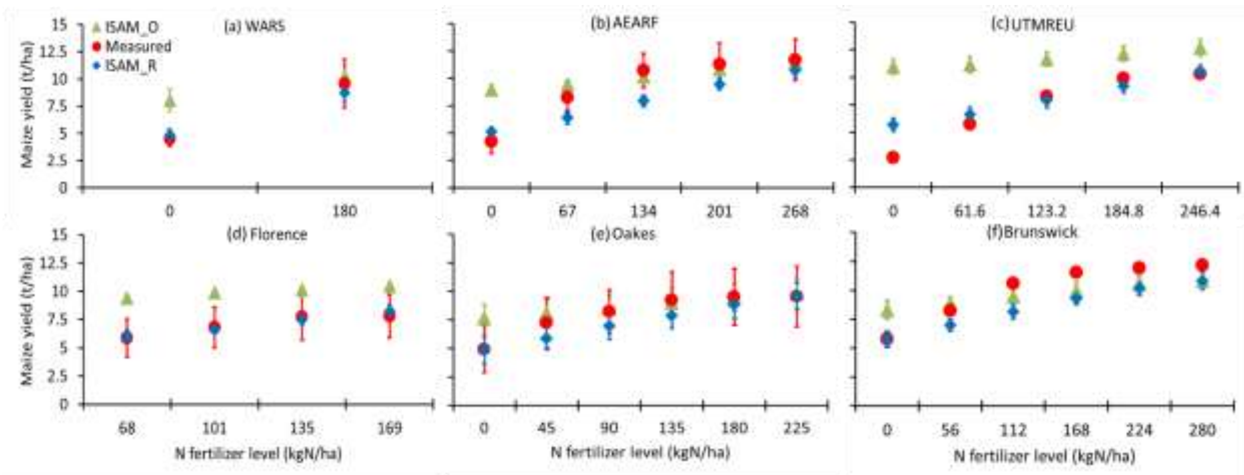

Figure S8a. Measured and simulated yields of maize with different N fertilizer levels at (a) WARS, (b) AEARF, (c) UTMREU, (d) Florence, (e) Oakes, and (f) Brunswick sites (Table S3). The red solid dots show measured values, green solid triangles show simulated results with original version of ISAM (ISAM_O), and blue solid diamonds for revised version of ISAM (ISAM_R). Bars show ± standard deviation indicating the temporal variability in measured yields of maize.

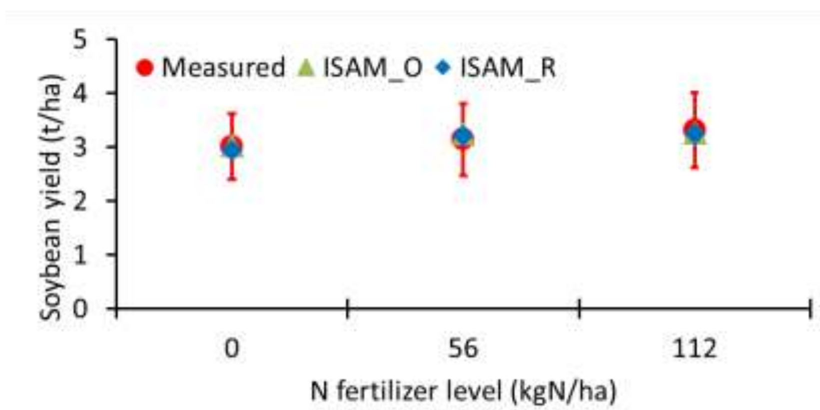

Figure S8b. Same as Figure S8a, but for soybean with different N fertilizer levels at University of Nebraska Field Laboratory, Mead site.

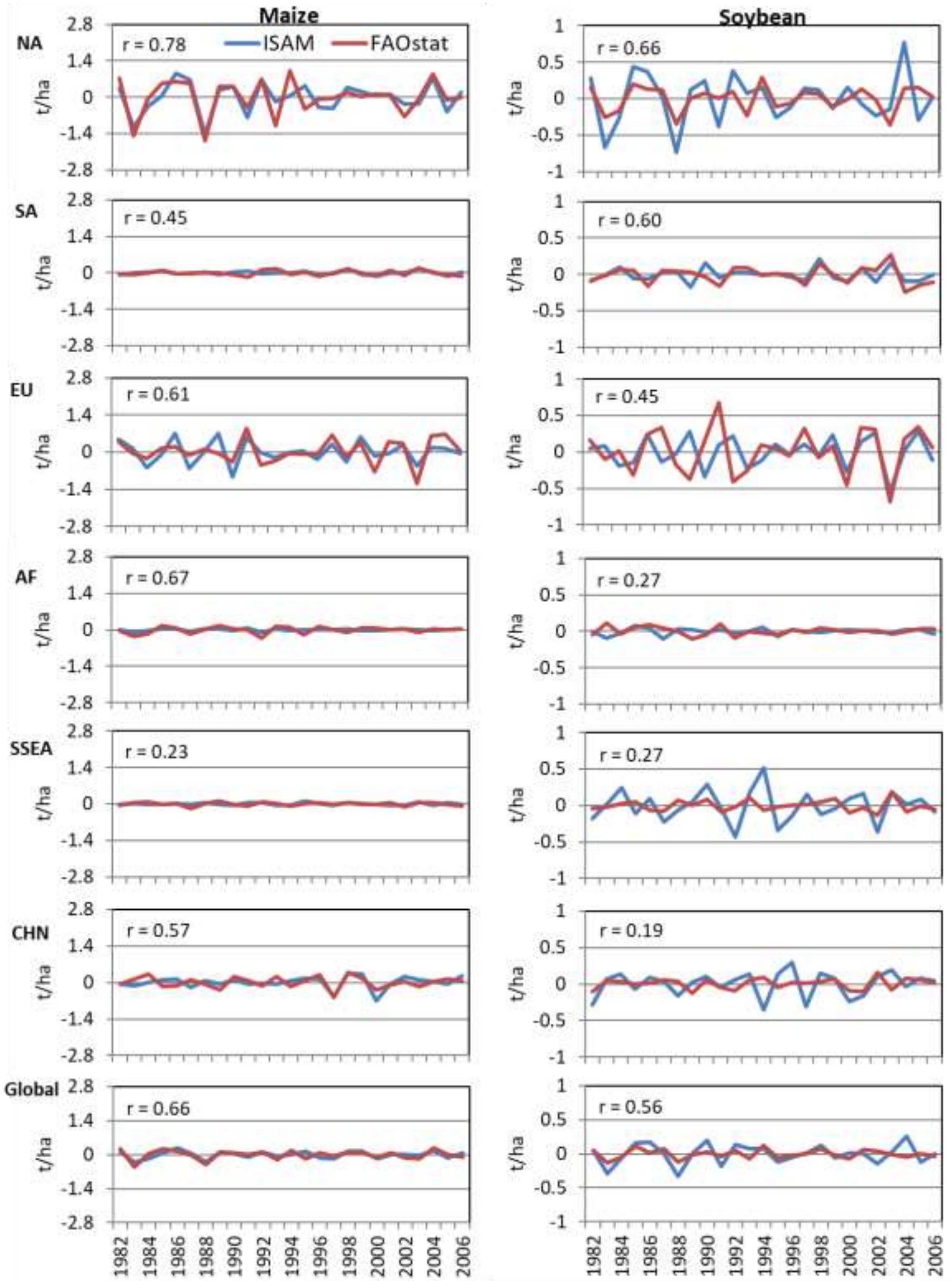
Maize
Soybean
ISAM
FAOstat
NA
SA
EU
AF
SSEA
CHN
Global
t/ha
r = 0.78
r = 0.66
r = 0.45
r = 0.60
r = 0.61
r = 0.45
r = 0.67
r = 0.27
r = 0.23
r = 0.27
r = 0.57
r = 0.19
r = 0.66
r = 0.56
2.8
1.4
0
-1.4
-2.8
1
0.5
0
-0.5
-1
1982
1984
1986
1988
1990
1992
1994
1996
1998
2000
2002
2004
2006

Figure S9. Comparision of ISAM estimated detrending maize (left panel), and soybean (right panel) yields (t/ha) for regional and global scale for the the period 1982-2006 with FAOstat data set. The "*r*" value in each figure is the correlation coefficient.

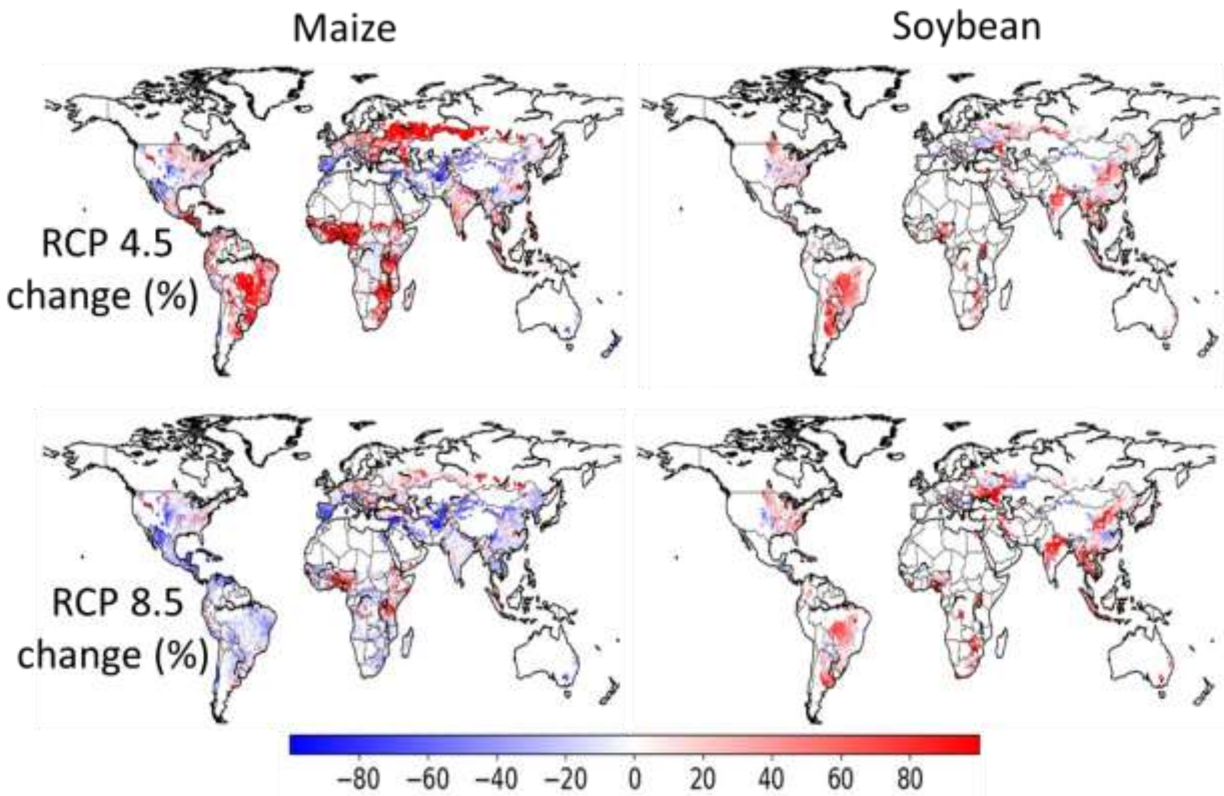

Figure S10. Maize (left panel) and soybean (right panel) changes in yields (%) for the 2090s relative to the 1996-2005 under RCP4.5 (top row) and RCP 8.5 scenarios (bottom row). Results are plotted at 0.5° x 0.5° degree spatial resolution.

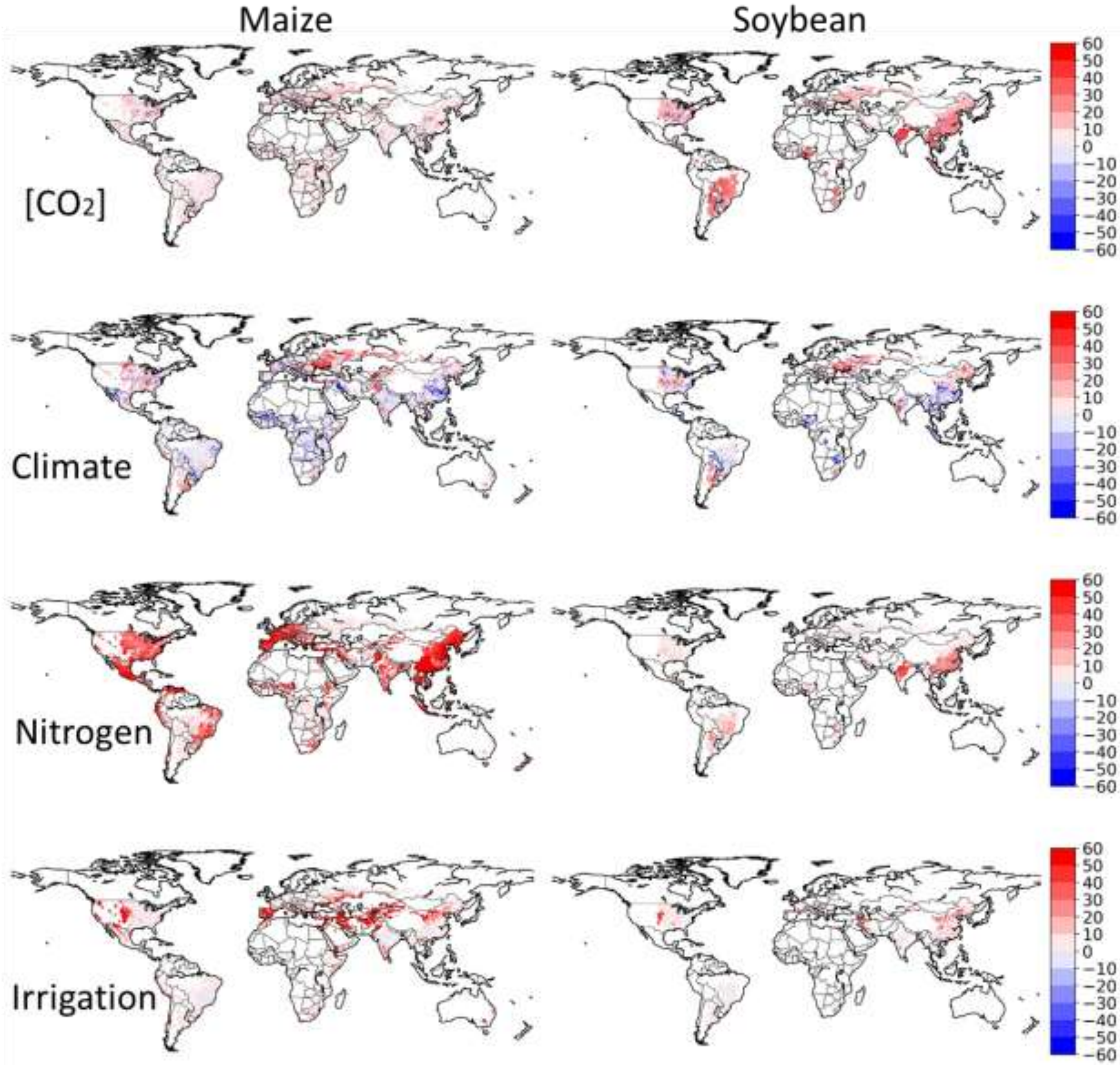

Figure S11a. Maize and soybean yield changes (%) averaged for 1996-2005 due to effects of CO_2, climate, irrigation and nitrogen inputfactors. Simulated areas are masked by crop-specific harvested areas averaged for 1996-2005.

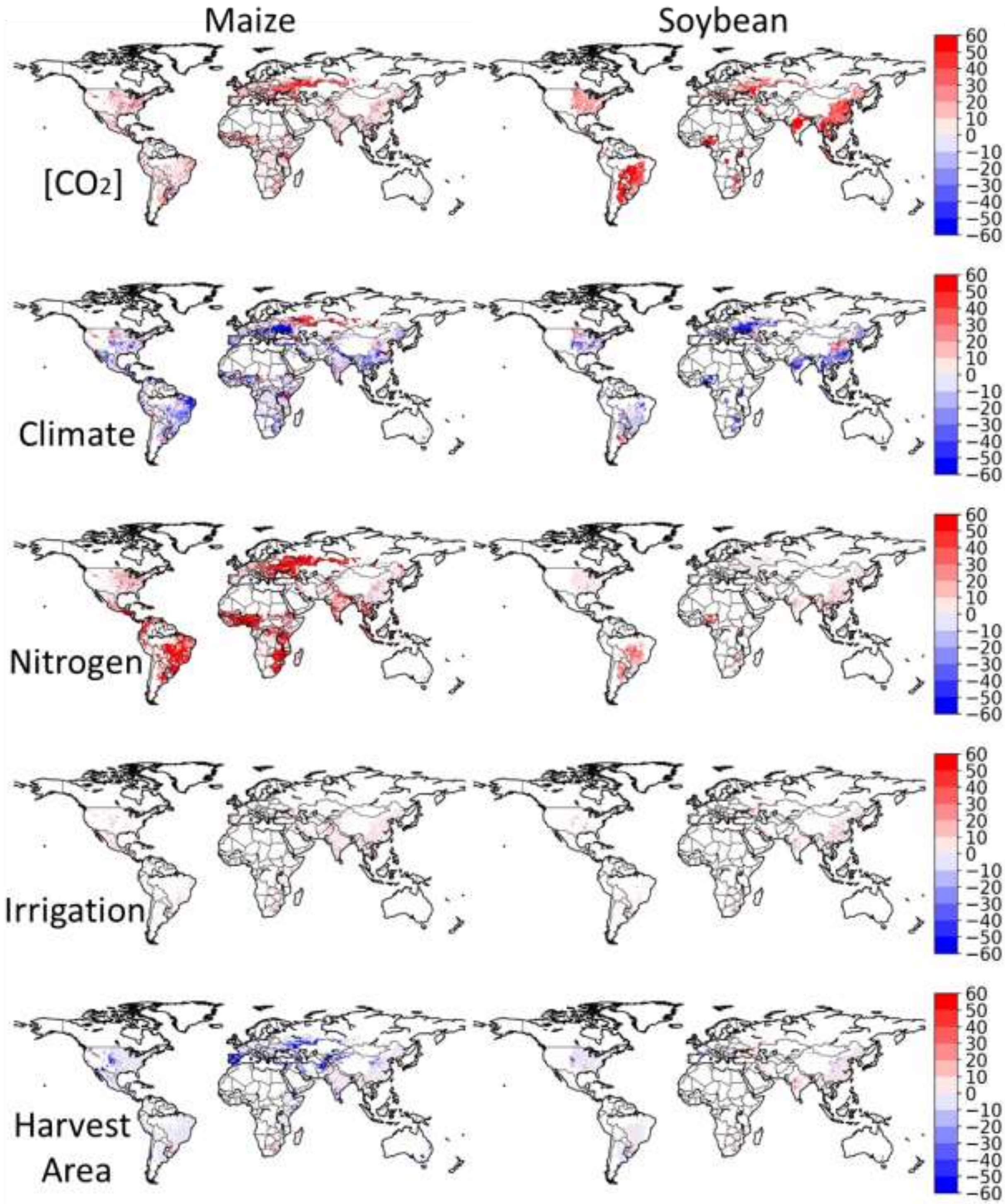

Figure S11b. Same as Figure S12a, but the changes (%) from 1996-2005 and to 2090s under RCP4.5.

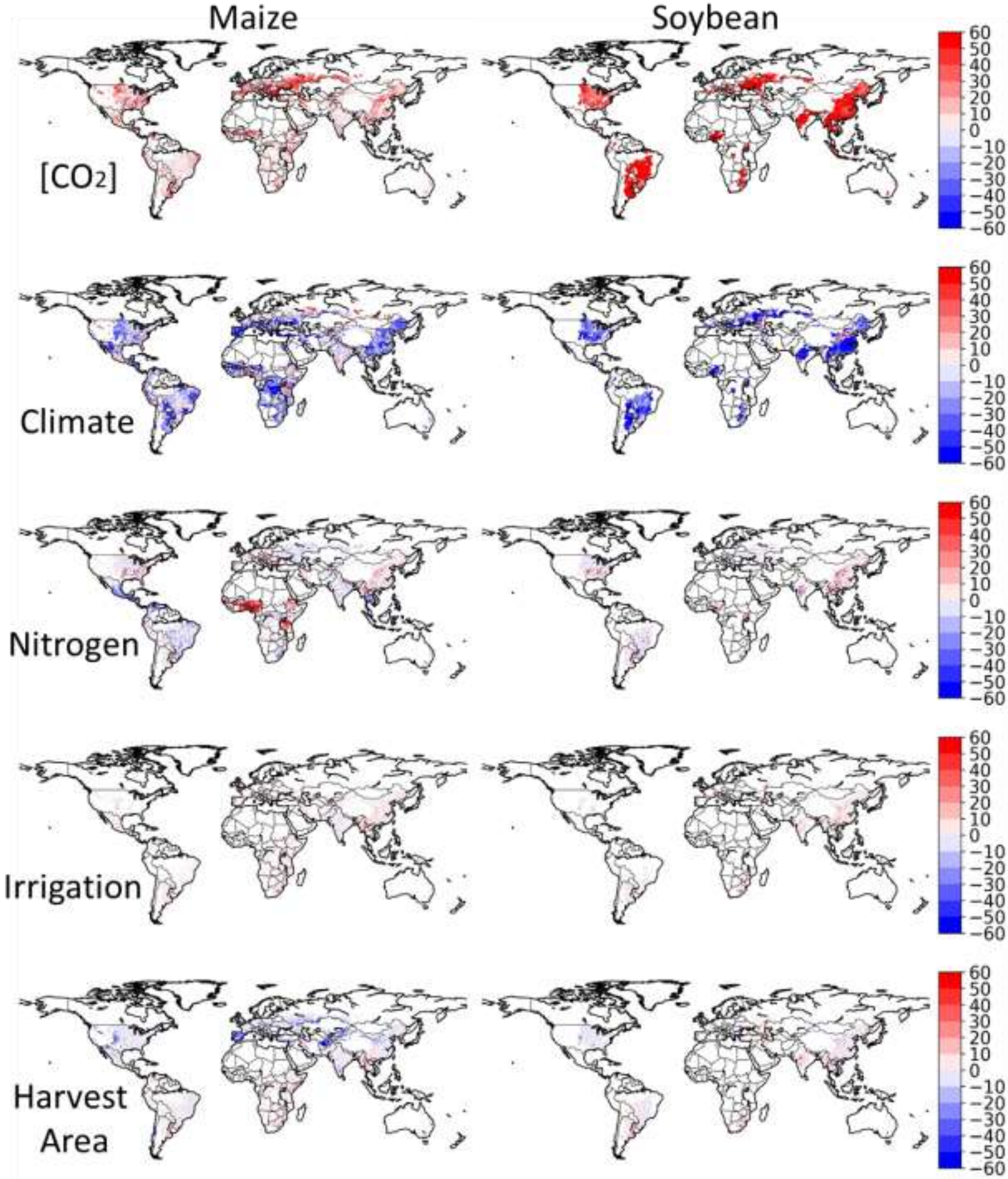

Figure S11c. Same as Figure S11a, but the changes (%) from 1996-2005 and to 2090s under RCP8.5.

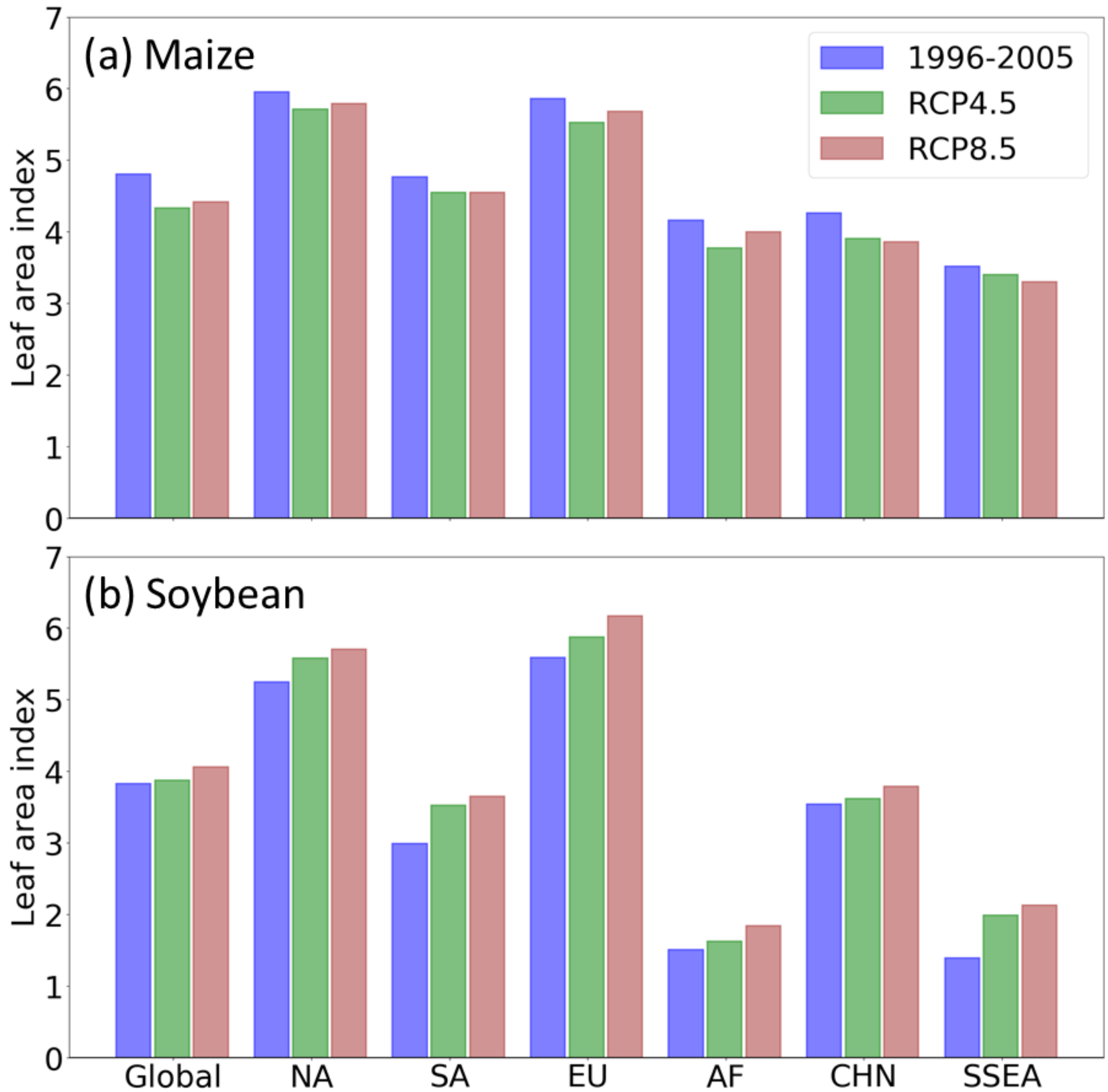

Figure S12. Peak leaf area index (LAI) for maize and soybean averged for 1996-2005 and 2090 under RCP 4.5 and RCP8.5 scenarios.

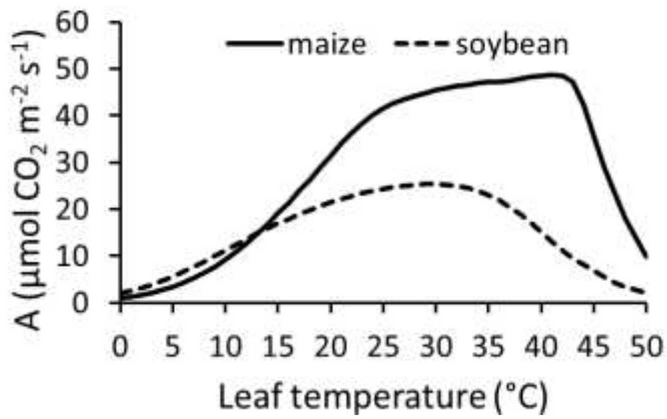

Figure S13 Simulated leaf net photosynthetic rates for C4 crops, maize and C3 crops, soybean response to leaf temperature. Solid line is maize and dashed line is soybean.

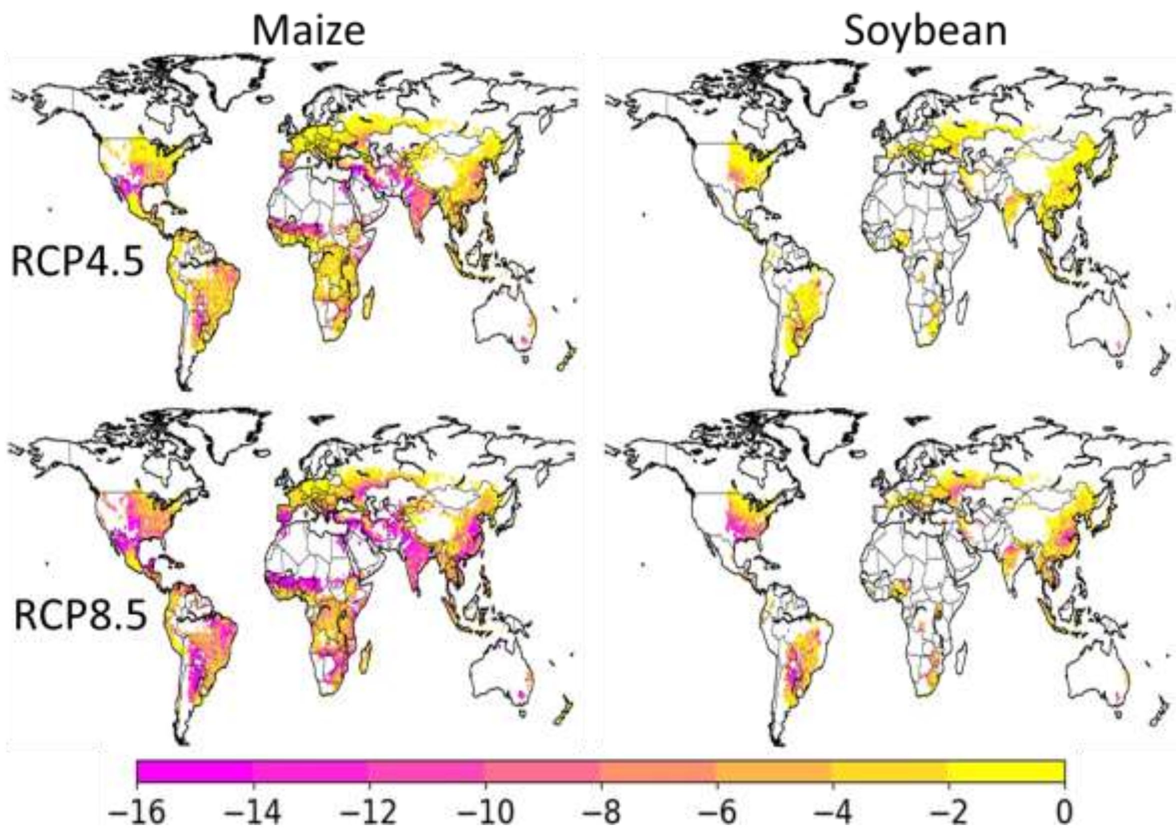

Figure S14. Maps of effect of heat stress on maize and soybean yield (%) for RCP4.5 and RCP8.5 in the 2090s. Values show (yield w/ heat stress minus yield w/o heat stress) / (yield w/o heat stress) *100%.

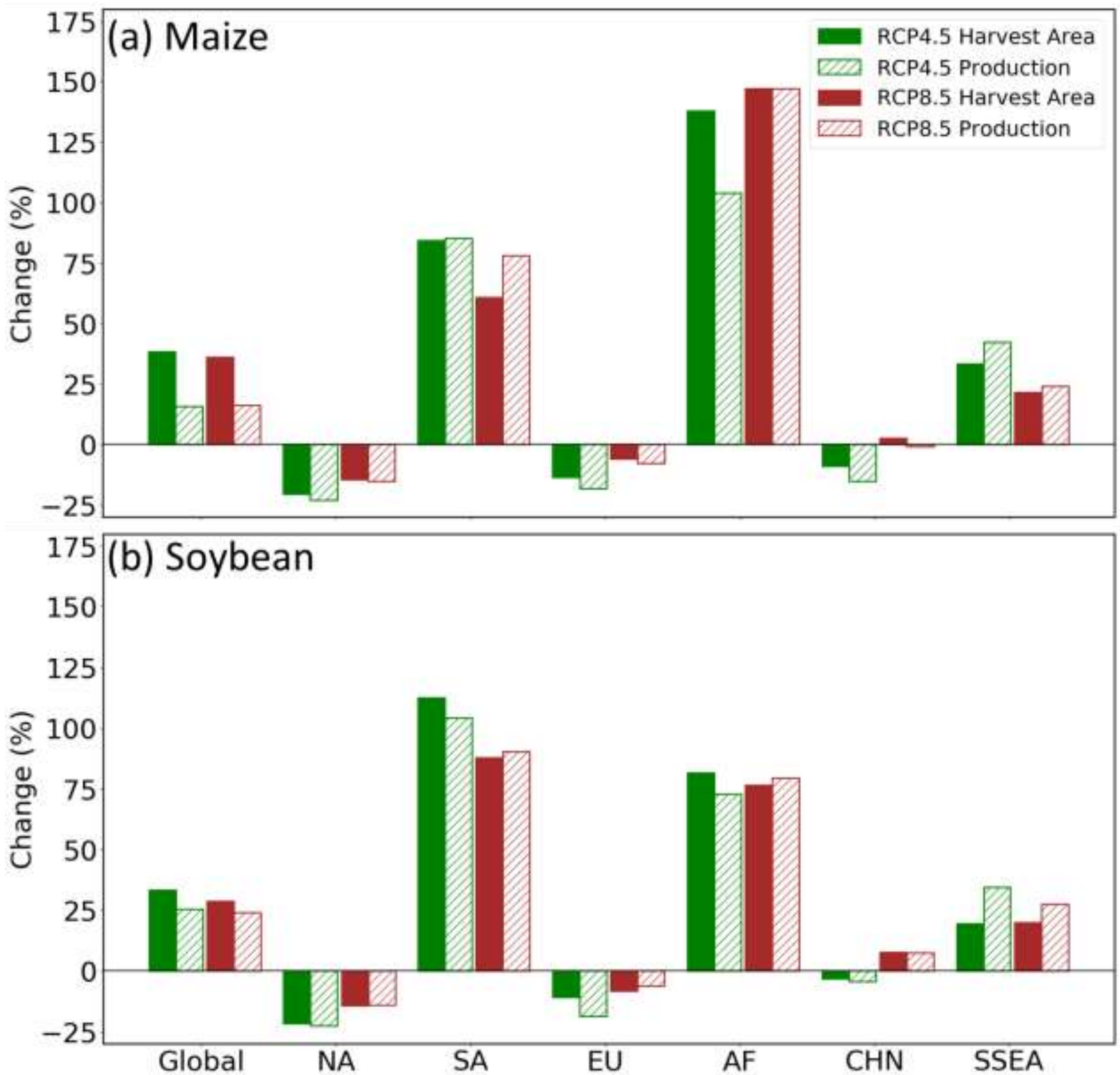

Figure S15. Changes in harvested areas (solid bars) and production (hatched bars) for (a) maize and (b) soybean under RCP4.5 and RCP8.5 scenarios (red bars) by the 2090s relative to the period of mean 1996-2005.

References

Akinnifesi, F. K., Makumba, W., Sileshi, G., Ajayi, O. C., & Mweta, D. (2007). Synergistic effect of inorganic N and P fertilizers and organic inputs from Gliricidia sepium on productivity of intercropped maize in Southern Malawi. *Plant and Soil*, *294*(1–2), 203–217. https://doi.org/10.1007/s11104-007-9247-z

Al-Ithawi, B., Deibert, E. J., & Olson, R. A. (1980). Applied N and Moisture Level Effects on Yield, Depth of Root Activity, and Nutrient Uptake by Soybeans1. *Agronomy Journal*, *72*(5), 827. https://doi.org/10.2134/agronj1980.00021962007200050031x

Alemayehu, Y., Shewarega, M., Resources, N., & Resources, N. (2015). Growth and Yield Responses of Maize (Zea Mays L .) to Different Nitrogen Rates under Rain-Fed Condition in Dilla Area , Southern, *5*(23), 40–46.

Arora, V. K. (2003). Simulating energy and carbon fluxes over winter wheat using coupled land surface and terrestrial ecosystem models. *Agricultural and Forest Meteorology*, *118*(1–2), 21–47. https://doi.org/10.1016/S0168-1923(03)00073-X

Attia, A., Shapiro, C., Kranz, W., Mamo, M., & Mainz, M. (2015). Improved Yield and Nitrogen Use Efficiency of Corn following Soybean in Irrigated Sandy Loams. *Soil Science Society of America Journal*, *79*(6), 1693. https://doi.org/10.2136/sssaj2015.05.0200

Bernacchi, C. J., Leakey, A. D. B., Heady, L. E., Morgan, P. B., Dohleman, F. G., McGrath, J. M., et al. (2006). Hourly and seasonal variation in photosynthesis and stomatal conductance of soybean grown at future CO2 and ozone concentrations for 3 years under fully open-air field conditions. *Plant, Cell and Environment*, *29*(11), 2077–2090. https://doi.org/10.1111/j.1365-3040.2006.01581.x

Bonan, G. B., Lawrence, P. J., Oleson, K. W., Levis, S., Jung, M., Reichstein, M., et al. (2011). Improving canopy processes in the Community Land Model version 4 (CLM4) using global flux fields empirically inferred from FLUXNET data, *116*, 1–22. https://doi.org/10.1029/2010JG001593

Boyer, C. N., Larson, J. A., Roberts, R. K., McClure, A. T., Tyler, D. D., & Zhou, V. (2013). Stochastic Corn Yield Response Functions to Nitrogen for Corn after Corn, Corn after Cotton, and Corn after Soybeans. *Journal of Agricultural and Applied Economics*, *45*(4), 669–681. https://doi.org/10.1017/s1074070800005198

De Bruin, J. L., & Pedersen, P. (2008). Effect of row spacing and seeding rate on soybean yield.

Agronomy Journal. https://doi.org/10.2134/agronj2007.0106

Chen, H., Dickinson, R. E., Dai, Y., & Zhou, L. (2011). Sensitivity of simulated terrestrial carbon assimilation and canopy transpiration to different stomatal conductance and carbon assimilation schemes. *Climate Dynamics*. https://doi.org/10.1007/s00382-010-0741-2

Déqué, M. (2007). Frequency of precipitation and temperature extremes over France in an anthropogenic scenario: Model results and statistical correction according to observed values. *Global and Planetary Change*. https://doi.org/10.1016/j.gloplacha.2006.11.030

Derby, N. E., Steele, D. D., Terpstra, J., Knighton, R. E., & Casey, F. X. M. (2005). Interactions of nitrogen, weather, soil, and irrigation on corn yield. *Agronomy Journal*, *97*(5), 1342–1351. https://doi.org/10.2134/agronj2005.0051

Deryng, D., Sacks, W. J., Barford, C. C., & Ramankutty, N. (2011). Simulating the effects of climate and agricultural management practices on global crop yield. *Global Biogeochemical Cycles*, *25*(2), n/a-n/a. https://doi.org/10.1029/2009GB003765

Deryng, D, Conway, D., Ramankutty, N., Price, J., & Warren, R. (2014). Global crop yield response to extreme heat stress under multiple climate change futures. *Environmental Research Letters*, *9*(3). https://doi.org/10.1088/1748-9326/9/3/034011

Deryng, D, Elliott, J., Folberth, C., Müller, C., Pugh, T. A. M., Boote, K. J., et al. (2016). Regional disparities in the beneficial effects of rising CO2 concentrations on crop water productivity. *Nature Climate Change*, *6*(8), 786–790. https://doi.org/10.1038/nclimate2995

Doraiswamy, P. C., McCarty, G. W., Hunt, E. R., Yost, R. S., Doumbia, M., & Franzluebbers, A. J. (2007). Modeling soil carbon sequestration in agricultural lands of Mali. *Agricultural Systems*. https://doi.org/10.1016/j.agsy.2005.09.011

Drewniak, B. A., Mishra, U., Song, J., Prell, J., & Kotamarthi, V. R. (2015). Modeling the impact of agricultural land use and management on US carbon budgets. *Biogeosciences*. https://doi.org/10.5194/bg-12-2119-2015

Dugje, I. Y., Omoigui, L. O., Ekeleme, F., Bandyopadhyay, R., Lava Kumar, P., & Kamara, a. Y. (2009). Farmers ' Guide to Soybean Production in Northern Nigeria, (May), 21.

Elliott, J., Müller, C., Deryng, D., Chryssanthacopoulos, J., Boote, K. J., Büchner, M., et al. (2015). The Global Gridded Crop Model Intercomparison: Data and modeling protocols for Phase 1 (v1.0). *Geoscientific Model Development*, *8*(2), 261–277. https://doi.org/10.5194/gmd-8-261-2015

Folberth, C., Gaiser, T., Abbaspour, K. C., Schulin, R., & Yang, H. (2012). Regionalization of a large-scale crop growth model for sub-Saharan Africa: Model setup, evaluation, and estimation of maize yields. *Agriculture, Ecosystems and Environment*, *151*, 21–33. https://doi.org/10.1016/j.agee.2012.01.026

Gabaldón-Leal, C., Webber, H., Otegui, M. E., Slafer, G. A., Ordóñez, R. A., Gaiser, T., et al. (2016). Modelling the impact of heat stress on maize yield formation. *Field Crops Research*. https://doi.org/10.1016/j.fcr.2016.08.013

Gehl, R. J., Schmidt, J. P., Maddux, L. D., & Gordon, W. B. (2005). Corn yield response to nitrogen rate and timing in sandy irrigated soils. *Agronomy Journal*, *97*(4), 1230–1238. https://doi.org/10.2134/agronj2004.0303

Getachew, M., & Belete, K. (2013). Yield Related Traits and Yield of Maize (Zea Mays L .) as affected by Green Manuring and Nitrogen Levels at Mizan Teferi , South-west. *Intl. J. Agron. Plant. Prod.*, *4*(7), 1462–1473.

Gray, S. B., Dermody, O., Klein, S. P., Locke, A. M., McGrath, J. M., Paul, R. E., et al. (2016). Intensifying drought eliminates the expected benefits of elevated carbon dioxide for soybean. *Nature Plants*, *2*, 1–26. https://doi.org/10.1038/nplants.2016.132

Hammad, H. M., Ahmad, A., Wajid, A., & Akhter, J. (2011). Maize response to time and rate of nitrogen application. *Pakistan Journal of Botany*, *43*(4), 1935–1942.

Hawkins, E., Osborne, T. M., Ho, C. K., & Challinor, A. J. (2013). Calibration and bias correction of climate projections for crop modelling: An idealised case study over Europe. *Agricultural and Forest Meteorology*, *170*, 19–31. https://doi.org/10.1016/j.agrformet.2012.04.007

Ho, C. K., Stephenson, D. B., Collins, M., Ferro, C. A. T., & Brown, S. J. (2012). Calibration strategies a source of additional uncertainty in climate change projections. *Bulletin of the American Meteorological Society*, *93*(1), 21–26. https://doi.org/10.1175/2011BAMS3110.1

Hurtt, G., Chini L., Sahajpal, R., Frolking S., et al. "Harmonization of global land-use change and management for the period 850-2100". *Geoscientific Model Development* (In prep).

Iizumi, T., Yokozawa, M., Sakurai, G., Travasso, M. I., Romanernkov, V., Oettli, P., et al. (2014). Historical changes in global yields: Major cereal and legume crops from 1982 to 2006. *Global Ecology and Biogeography*, *23*(3), 346–357.

https://doi.org/10.1111/geb.12120

Kucharik, C. J., & Brye, K. R. (2003). Integrated biosphere simulator (IBIS) yield and nitrate loss predictions for Wisconsin maize receiving varied amounts of nitrogen fertilizer. *Journal of Environmental Quality*, *32*(1), 247–268.

Lamarque, J. F., Kyle, P. P., Meinshausen, M., Riahi, K., Smith, S. J., van Vuuren, D. P., et al. (2011). Global and regional evolution of short-lived radiatively-active gases and aerosols in the Representative Concentration Pathways. *Climatic Change*. https://doi.org/10.1007/s10584-011-0155-0

Leng, G., Huang, M., Tang, Q., & Leung, L. R. (2015). A modeling study of irrigation effects on global surface water and groundwater resources under a changing climate. *Journal of Advances in Modeling Earth Systems*. https://doi.org/10.1002/2015MS000437

Liu, J., You, L., Amini, M., Obersteiner, M., Herrero, M., Zehnder, A. J. B., & Yang, H. (2010). A high-resolution assessment on global nitrogen flows in cropland. *Proceedings of the National Academy of Sciences*, *107*(17), 8035–8040. https://doi.org/10.1073/pnas.0913658107

Manderscheid, R., Erbs, M., & Weigel, H. (2014). Interactive effects of free-air CO 2 enrichment and drought stress on maize growth. *European Journal of Agronomy*, *52*, 11–21. https://doi.org/10.1016/j.eja.2011.12.007

Monfreda, C., Ramankutty, N., & Foley, J. A. (2008). Farming the planet: 2. Geographic distribution of crop areas, yields, physiological types, and net primary production in the year 2000. *Global Biogeochemical Cycles*, *22*(1), 1–19. https://doi.org/10.1029/2007GB002947

Morgan, P. B., Bollero, G. A., Nelson, R. L., Dohleman, F. G., & Long, S. P. (2005). Smaller than predicted increase in aboveground net primary production and yield of field-grown soybean under fully open-air [CO 2] elevation. *Global Change Biology*, *11*(10), 1856–1865. https://doi.org/10.1111/j.1365-2486.2005.001017.x

Moriondo, M., Giannakopoulos, C., & Bindi, M. (2011). Climate change impact assessment: The role of climate extremes in crop yield simulation. *Climatic Change*, *104*(3–4), 679–701. https://doi.org/10.1007/s10584-010-9871-0

Mueller, N. D., Gerber, J. S., Johnston, M., Ray, D. K., Ramankutty, N., & Foley, J. A. (2012). Closing yield gaps through nutrient and water management. *Nature*.

https://doi.org/10.1038/nature11420

Müller, C., Elliott, J., Chryssanthacopoulos, J., Arneth, A., Balkovic, J., Ciais, P., et al. (2017). Global gridded crop model evaluation: Benchmarking, skills, deficiencies and implications. *Geoscientific Model Development*. https://doi.org/10.5194/gmd-10-1403-2017

Müller, C., Elliott, J., Kelly, D., Arneth, A., Balkovic, J., Ciais, P., et al. (2019). The Global Gridded Crop Model Intercomparison phase 1 simulation dataset, 1–22. https://doi.org/10.1038/s41597-019-0023-8

M'Po, Y. N. T., Lawin, A.E., Oyerinde, G.T., Yao, B.K., & Afouda, A.A (2016). Comparison of Daily Precipitation Bias Correction Methods Based on Four Regional Climate Model Outputs in Ouémé Basin, Benin. *Hydrology*. https://doi.org/10.11648/j.hyd.20160406.11

Nangia, V., Turral, H., & Molden, D. (2008). Increasing water productivity with improved N fertilizer management. *Irrigation and Drainage Systems*, *22*(3–4), 193–207. https://doi.org/10.1007/s10795-008-9051-9

Oleson, K. W., Lawrence, D. M., Bonan, G. B., Drewniak, B., Huang, M., Charles, D., et al. (2013). NCAR/TN-503+STR NCAR Technical Note (July 2013).

Portmann, F. T., Siebert, S., & Döll, P. (2010). MIRCA2000-Global monthly irrigated and rainfed crop areas around the year 2000: A new high-resolution data set for agricultural and hydrological modeling. *Global Biogeochemical Cycles*. https://doi.org/10.1029/2008gb003435

Puntel, L. A., Sawyer, J. E., Barker, D. W., Dietzel, R., Poffenbarger, H., Castellano, M. J., et al. (2016). Modeling Long-Term Corn Yield Response to Nitrogen Rate and Crop Rotation, *7*(November), 1–18. https://doi.org/10.3389/fpls.2016.01630

Ren, X., Weitzel, M., O'Neill, B. C., Lawrence, P., Meiyappan, P., Levis, S., et al. (2018). Avoided economic impacts of climate change on agriculture: integrating a land surface model (CLM) with a global economic model (iPETS). *Climatic Change*, *146*(3–4), 517–531. https://doi.org/10.1007/s10584-016-1791-1

Sacks, W. J., Deryng, D., Foley, J. A., & Ramankutty, N. (2010). Crop planting dates: An analysis of global patterns. *Global Ecology and Biogeography*, *19*(5), 607–620. https://doi.org/10.1111/j.1466-8238.2010.00551.x

Sellers, P. J., Los, S. O., Tucker, C. J., Justice, C. O., Dazlich, D. A., Collatz, G. J., & Randall, D. A. (1996). A revised land surface parameterization (SiB2) for atmospheric GCMs. Part

II: The generation of global fields of terrestrial biophysical parameters from satellite data. *Journal of Climate*. https://doi.org/10.1175/1520-0442(1996)009<0706:ARLSPF>2.0.CO;2

Shangguan, W., Dai, Y., Duan, Q., Liu, B., & Yuan, H. (2014). A global soil data set for earth system modeling. *Journal of Advances in Modeling Earth Systems*. https://doi.org/10.1002/2013MS000293

Sharma, P. & Jain, A. K. (2018). Assessing the effects of land use changes, nitrogen fertilizer application and deposition on nitrogen leaching in South and South East Asia. AGU Fall Meeting Abstract.

Siebert, S., Ewert, F., Eyshi Rezaei, E., Kage, H., & Graß, R. (2014). Impact of heat stress on crop yield - On the importance of considering canopy temperature. *Environmental Research Letters*. https://doi.org/10.1088/1748-9326/9/4/044012

Song, Y., Jain, A. K., & McIsaac, G. F. (2013). Implementation of dynamic crop growth processes into a land surface model: Evaluation of energy, water and carbon fluxes under corn and soybean rotation. *Biogeosciences*, *10*(12), 8039–8066. https://doi.org/10.5194/bg-10-8039-2013

Song, Y, Jain, A. K., Landuyt, W., Kheshgi, H. S., & Khanna, M. (2015). Estimates of Biomass Yield for Perennial Bioenergy Grasses in the USA. *Bioenergy Research*, *8*(2), 688–715. https://doi.org/10.1007/s12155-014-9546-1

Song, Y, Cervarich, M., Jain, A. K., Kheshgi, H. S., Landuyt, W., & Cai, X. (2016). The Interplay Between Bioenergy Grass Production and Water Resources in the United States of America. *Environmental Science & Technology*, *50*(6), 3010–3019. https://doi.org/10.1021/acs.est.5b05239

Stehfest, E., Heistermann, M., Priess, J. A., Ojima, D. S., & Alcamo, J. (2007). Simulation of global crop production with the ecosystem model DayCent. *Ecological Modelling*, *209*(2–4), 203–219. https://doi.org/10.1016/j.ecolmodel.2007.06.028

Stone, K. C., Camp, C. R., Sadler, E. J., Evans, D. E., & Millen, J. A. (2010). Corn Yield Response to Nitrogen Fertilizer and Irrigation in the Southeastern Coastal Plain. *Applied Engineering in Agriculture*, *26*(3), 429–438.

Teixeira, E. I., Fischer, G., Van Velthuizen, H., Walter, C., & Ewert, F. (2013). Global hot-spots of heat stress on agricultural crops due to climate change. *Agricultural and Forest Meteorology*, *170*, 206–215. https://doi.org/10.1016/j.agrformet.2011.09.002

Twine, T. E., Bryant, J. J., T. Richter, K., Bernacchi, C. J., Mcconnaughay, K. D., Morris, S. J., & Leakey, A. D. B. (2013). Impacts of elevated CO2 concentration on the productivity and surface energy budget of the soybean and maize agroecosystem in the Midwest USA. *Global Change Biology*, *19*(9), 2838–2852. https://doi.org/10.1111/gcb.12270

United States Department of Agriculture, Natural Resources Conservation Service. (2019). Soil Survey Geographic (SSURGO) Database. Available online at https://sdmdataaccess.sc.egov.usda.gov. Accessed [May 2019].

VANLOOCKE, A., BERNACCHI, C. J., & TWINE, T. E. (2010). The impacts of Miscanthus×giganteus production on the Midwest US hydrologic cycle. *GCB Bioenergy*. https://doi.org/10.1111/j.1757-1707.2010.01053.x

Verma, S. B., Dobermann, A., Cassman, K. G., Walters, D. T., Knops, J. M., Arkebauer, T. J., et al. (2005). Annual carbon dioxide exchange in irrigated and rainfed maize-based agroecosystems. *Agricultural and Forest Meteorology*, *131*(1–2), 77–96. https://doi.org/10.1016/j.agrformet.2005.05.003

Waha, K., Van Bussel, L. G. J., Müller, C., & Bondeau, A. (2012). Climate-driven simulation of global crop sowing dates. *Global Ecology and Biogeography*, *21*(2), 247–259. https://doi.org/10.1111/j.1466-8238.2011.00678.x

Webber, H., Martre, P., Asseng, S., Kimball, B., White, J., Ottman, M., et al. (2017). Canopy temperature for simulation of heat stress in irrigated wheat in a semi-arid environment: A multi-model comparison. *Field Crops Research*, *202*, 21–35. https://doi.org/10.1016/j.fcr.2015.10.009

You, L., Wood, S., Wood-Sichra, U., & Wu, W. (2014). Generating global crop distribution maps: From census to grid. *Agricultural Systems*, *127*, 53–60. https://doi.org/10.1016/j.agsy.2014.01.002